國立交通大學

電子物理研究所

碩士論文

# 局域聲子在低維度的介觀物理系統中對量子傳輸的影響

# LOCAL PHONON EFFECTS IN LOW DIMENSION MESOSCOPIC STRUCTURES

研 究 生：林哲民

指導教授：朱仲夏 博士

中華民國九十四年7月

# 局域聲子在低維度的介觀物理系統中對量子傳輸的影響

# LOCAL PHONON EFFECTS IN LOW DIMENSION MESOSCOPIC STRUCTURES


研 究 生：林哲民　　Student: J. M. Lin

指導教授：朱仲夏　　Advisor: C. S. Chu

國立交通大學

電子物理研究所


碩士論文

A Thesis
Submitted to Institute of Electrophysics
College of Science
National Chiao Tung University
In partial Fulfillment of the Requirements
for the Degree of
Master
In

Electrophysics

July 2005
Hsinchu, Taiwan, Republic of China

中 華 民 國 九 十 四 年 七 月

# 局域聲子在低維度的介觀物理系統中對量子傳輸的影響

研究生：林哲民　　指導教授：朱仲夏　博士

國立交通大學電子物理研究所

## 摘　　要

本論文的研究主要有兩個主題，第一個室探討局域聲子(local phonon)對單電子在一維導線中對量子傳輸特性的影響，第二個是探討當單電子透射(tunnel)位於一維導線中量子點(quantum dot)中局域聲子所產生的影響。在第一個主題中，我們對系統作了許多細節的探討來當作我們研究第二個主題的基礎，包括局域聲子的吸引性或排斥性（attractive or repulsive），聲子溫度（phonon temperature），局域聲子的頻率和重量對單電子在一維導線中傳輸特性的影響 。在第二個主題中，因為我們考慮在局域聲子的影響下量子點的傳輸特性，我們可以將電子侷限在量子點中來使電子的波長變短到可以跟聲子波長可以比較的長度，而且我們可以藉由這各方法來增強聲子側能帶( phonon sideband)效應。

# LOCAL PHONON EFFECTS IN LOW DIMENSION MESOSCOPIC STRUCTURE

Student: Jer-Ming Lin Advisor: Dr. Chon-Saar Chu

Department of Electrophysics

National Chiao-Tung University

## Abstract

There are two main topics in our thesis. First, we study the effect of local phonons on the quantum transport in a 1-D wire. Second, we investigate the effect of local phonons on the single electron tunneling through a quantum dot. In the first topic, we take deep insight to our system including the attractive or repulsive local phonons, the effect of phonon temperature *T,* oscillating frequency of local phonons $\omega$, and mass of local phonon *M*. Take the analyses made in the first topic as a basis. In the second topic, because we study quantum transport properties of a single-molecular quantum dot w with local phonon effect, we can confine the incident electron in the quantum dot to shorten its wavelength, which can be compared to the phonon wavelength at ground state. And, we can enhance the phonon sideband effects by this way.

# 誌謝

從專題生開始，就接受老師得指導，謝謝老師這三年來的指導，除了專業上的指導外，也謝謝老師傳達給我對於物理的熱情，作研究的方法與態度。除此之外，最想感謝的是王率堯學長，所有研究的細節和學長的友情都是我最想感謝的。也謝謝唐志雄和鄔其君學長許許多多寶貴的意見和指導。當然也謝謝實驗室的同學，敬航、育佑、淑娟、宇廷，有你們的陪伴這兩年才不會這麼孤單，最後當然謝謝爸爸、媽媽，謝謝你們從小到大的扶養與栽培。

# Contents

# List of Figures

# Chapter 1

# Introduction

## 1.1 Introduction

The advancement of fabrication techniques and theoretical development of quantum transport in mesoscopic nanostructures has provided great potential to the development of novel quantum devices in nanoscale, quantum wires and quantum rings for example. One of the interesting studies in mesoscopic systems is the effects due to electron- phonon interaction. Recently, solvable models for the interaction of phonons with electrons in quantum dot [1] and quasi-one-dimensional system [2,3] have been explored by several groups. In the work of Gelfand et a*l.* [2], they invoked an ad-hoc electron-local phonon interaction Hamiltonian $H_{ij}(t) = -t_{ij} + \delta_{ij}\,[V_{0i} + V_{1i}(t)]$ within a tight-binding model. The static barrier and the local phonons, with $V_{1i}(t) = V_1 \delta_{i0}\,[be^{-i\omega t} + b^{+}e^{i\omega t}]$, are located at i=0 without center-mass-variation. Naturally, we may ask: what about center-mass-variation local phonons? Therefore, in Ch. 4, we consider a simple model to study the effect of local phonons on the transport characteristics in a one-dimensional system. The local phonons is modeled by an impurity which center is allowed to oscillate about its equilibrium position with a frequency $\omega$. By treating the dynamics of both the electron and the impurity in the same footing, we aim at looking into detail of the transport characteristics of the electron.

In addition to these semiconductor devices, molecular devices also attract more and more attention to study their transport properties both in experimently and theorically, including single molecule devices [4-11], nanocrystals[14-18], and

nanotubes[19-20]. Especially the single molecular device experimental results worked by H. Park. *et al.* [5] show the evidence of conductance peak due to $C_{60}$' center-mass-variation, which we will introduce in Sec. 2.2 and 2.2. Take the analysis made in Ch. 4 as basis, we try to construct a brief model to describe this phenomenon. Therefore, In Ch. 5, we study the transport characteristics of the electron resonant tunneling through a single-molecular quantum dot coupled with center-mass-oscillation local phonons with non-perturbed method. As expected, it is found that in the presence of electron-phonon coupling, in addition to the resonance peak associated with the resonance level of the dot, phonon sideband peaks with the separation set by phonon energy $\hbar\omega$ in the conductance. What is the interesting is that we can enhance the phonon sideband structures by confine the incident electron in the dot the reduce its wavelength which can be compared with the wavelength of local phonon at ground state in contrast to the 1-D wire model studied in Ch. 4.

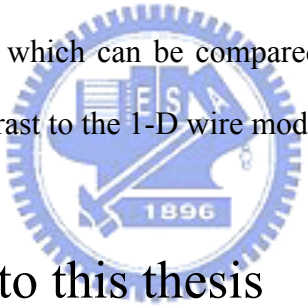

## 1.2A guiding tour to this thesis

Thus far we have not yet provided the scaling of mesoscopic physics which is quite different from the devices having larger scale. This will be covered in Sec. 1.3. In Ch. 2, we introduce the quantized conductance phenomenon, which is a important characteristics of the mesoscopic system. In addition, the possible application of our study " single molecule device" is briefly presented including the process of fabrication and some experimental results extracted from the works of M. A. Reed *et al.* [4], and H. park *et al.* [5]. In chapter 3, we introduce the Landauer-Büttiker formalism and scattering matrix method. We follow these methods to complete our theoretical calculation in Ch. 4 and Ch.5.

The numerical results, discussion, and theoretical calculation of the effect of

local phonons on the transport characteristics in a one-dimensional quantum channel and the transport characteristics of the electron resonant tunneling through a quantum dot coupled with local phonons are respectively shown in Ch. 4. and Ch. 5. Finally, we conclude our results and mention a few feasible direction of our future work.

# 1.3 Length Scale

A tiny circuit with dimension between microscopic and macroscopic is so called mesocsopic. The length scale of a mesoscopic system greater than microscopic's, like atom, but smaller than the macroscopic regime, like bulk.

A system shows quantum behavior if its dimensions is comparable to three characteristic length scales (1) the Fermi wavelength, (2) the mean free path, and (3) the phase relaxation length which we will illustrate as follow. However, in the mesoscopic regime, the phase coherence of the charge carriers is preserved within the entire system.

First, let's see the Fermi wave length. The Fermi wavelength is written as

$$\lambda_f = 2\pi/k_F = (2\pi n_s)^{1/2} .$$

For an high electron density of $5\times10^{11}/cm^2$, the Fermi wave length is about 35nm at sufficient low temperatures.

Second, the mean free path ($l_m$) can be defined as

$$l_m = \nu_F \tau_m .$$

where the time scale $\tau_m$ give us the average time interval which refers to an electron in a perfect crystal with large momentum changes, for example collision with impurities . Then the momentum relaxation time $\tau_m$ can be relaxted to yhe collision time $\tau_c$ by

$$\frac{1}{\tau_m} = \frac{\alpha_\varphi}{\tau_c} \quad ,$$

where $\alpha_\varphi$ denotes the effectiveness of an individual collision in destroying phase. The phase breaking length is given by

$$l_\varphi = \nu_F \quad \tau_{\varphi.}$$

Further, $L_\varphi$ is the length scale over, which the electron stay in the same eigenstate which would be destroyed by phonons, spin-orbit, scattering, et al.

Thanks to the maturity of the nanotechnology, the $L_\varphi$ in weakly disordered can be longer than the dimension size of channel's width and length. Therefore, we can see more further physical interesting characteristics in this regime.

Finally, we talk about the difference between ballistic and diffusive regime. The ballistic regime means that the phase-breaking time is shorter than the momentum relaxation time and cause $l_{\mathrm{m}} > l_\varphi > L$(channel length). However, in the diffusive regime($l_\varphi > l_{\mathrm{m}} > L$) , the momentum relaxation time is shorter than the phase relaxation time. Therefore, the motion of an electron is not ballistic over a phase-relaxation time.

# Chapter 2

# Experimental Technologies

## 2.1 Conductance quantization

The low temperature quantized conductance of narrow split-gate Quantum-point-contacts(QPCS) model from GaAs-$Al_xGa_{1-x}As$ heterostructures was independently discovered by the B. J. van Wees *et al*. [12] and D.Wharam *et al*. [13]. It is one of the most interesting discovery in mesoscopic history.

Because the point contact studied by B. J. van Wees of width and length $L$ much smaller than mean free path $l_m$ = 8.5 μm. We can view it as the ballistic regime. In this regime, they discovered a sequence of steps of the voltage of the split gate as shown in Fig 2.1.

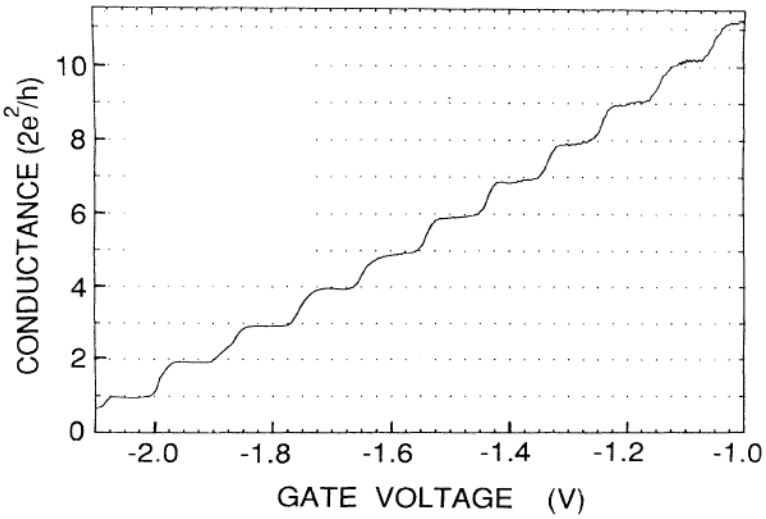


Fig 2.1 : Conductance is plotted against gate voltage experimentally by B. J. van Wees *et al.* [12]

As we can see, the conductance is quantized in units of $2e^2/h$. This result relies

on the fact of increase in number of propagating modes. Besides, it also can be seen as a special case of Landauer-Bütikker formula $G = 2e^2 / h \sum_{n,m} T_{n,m}$ with no channel mixing.

For the case of the hard wall modeling the transverse confinement to explain the experiment's result more clear. The dispersion relation *E(n, k)* can be written as *E(n, k)* = $(n\pi/w)^2 + k^2$ , where we have set $\hbar^2/2m = 1$. And the cut-off energy of hard wall confinement is $\varepsilon(n) = (n\pi/w)^2$ . The number of transverse modes contributes to the conductance at energy E is obtained by counting the number of modes having cut-off energies smaller than E. Therefore, if we change the voltage to cause the electrochemical potential μ to vary from $\varepsilon(2) \geq \mu \geq \varepsilon(1)$ to $\varepsilon(3) \geq \mu \geq \varepsilon(2)$, more electron channels open to propagate and contribute contributing to conductance. The conductance *G* will accordingly be changed from $G = 2e^2/h$ to $G = 4e^2/h$.

# 2.2 Experimental Application

## 2.2.1 Single-molecular Transistor Device

Here we report the fabrication and some experiment's result of metal-molecule-metal device seen Fig 2.2. Such measurements are experimentally challenging and intriguing because one can test the validity of transport approximations at the molecule level. Such a metal-molecule-metal configuration would be to connect a single molecuke between metallic contacts. Such a metal-molecule-metal configuration would present the molecular embodiment of a system analogous to a quantum dot; with the potential barrier of the semiconductor system being replaced by any existing contact barrier of the molecule-metal interface.

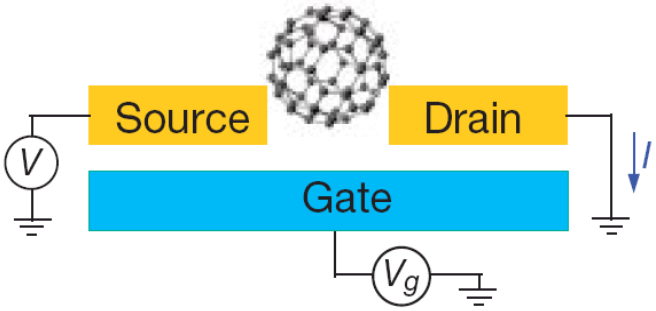


Fig 2.2 Single-molecular device extracted from H. Park. *et al*.[5].

## 2.2.2 Fabrication of Single-molecular device

In this section, we list a serious of pictures as shown in Fig 2.2 to roughly illustrate the "break junction method " which fabricating metal-molecule-metal device extracted from Reference [4].

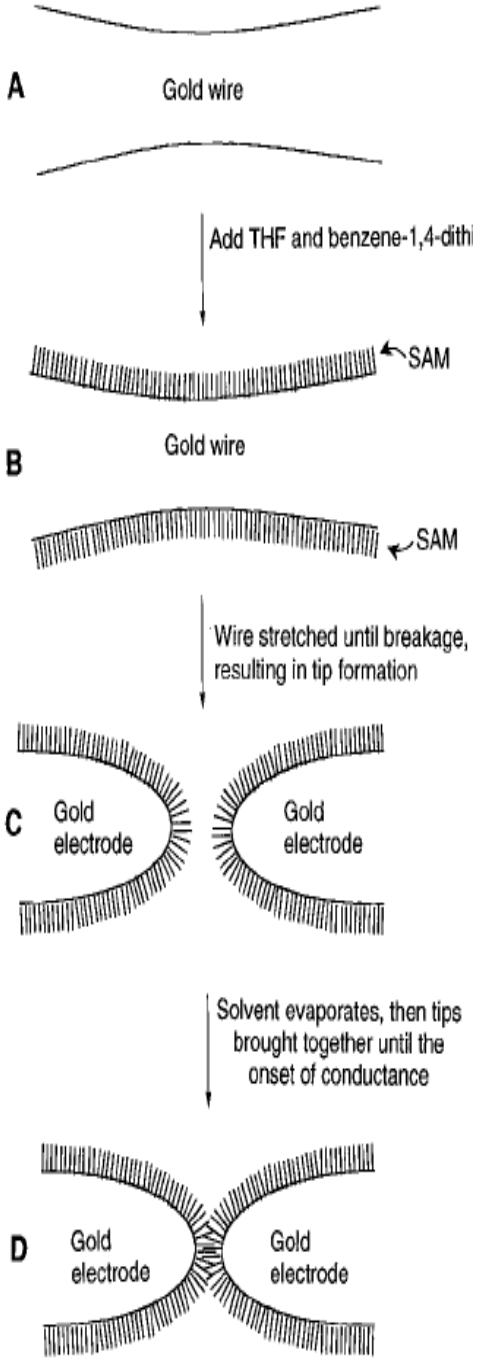


Fig 2.3 Fabrication process of single molecular device extracted from M. A. Reed *et al.* [4]

In Figure 2.3.A, the authors prepare a metal wire, a gold wire for example, glued on to a flexible substrate. In Figure 2.3.B, they add the organic resolution to the gold wire. In this case, they use the benzene-1,4-dithiol in tetrahydrofuran(THF). Besides, they also can use a dilute toluene of $C_{60}$ [5]. Then, they can get a self-assembled

monolayer on the gold wire surface. In Fig 2.3.C, they mechanically stretched the wire and make the breakage of the gold wire producing two opposing gold electrodes with SAM-covered and we can get a pair of atomically sharp contacts. Last, in Fig 2.3.D ,as the solvent evaporate, the two contacts will slowly move together. And, they will keep moving until we get the onset of conductance.

## 2.2.3 Recent Experimental results of Single-molecular device

In this section, we illustrate some interesting experimental results shown in Fig2.4 and Fig 2.5 measured by H. Park et a*l*. [5]. In H. Park et al.'s work, they fabricate a single-molecule transistors based individual $C_{60}$ molecules connected to gold electrodes. And in their experimental results show the evidence for a coupling between the center-of-mass motion of the $C_{60}$ molecules and single-electron hopping. Fig 2.4 is two-dimensional conductance ($\partial I/\partial V$) plotting as a function of the bias voltage(V) and the gate voltage($V_g$). Data were obtained from four different devices prepared from separated fabrication runs. The dark triangular regions correspond to the conductance gap, and bright lines represent peaks in the differential conductance. In fig 2.4 (a)-(d), they can obviously find the conductance gap arising from the energy required to add(remove) an electron to(from) $C_{60}$. And they define the gate voltage which the conductance gap disappears is $V_c$ where the total energy of the system is same for two different $C_{60}$ charge states. In addition to the conductance gap phenomenon, the white arrow indicate the $\partial I/\partial V$ peaks appear when a new quantized excitation becomes energetically accessible, providing an electron-tunneling pathway between $C_{60}$ and the gold electrodes. The exact energy value of these quantized excitations which can be determined from the bias voltage intercepting the conductance gap varied from device to device and ranged from 3 to 7 meV.

Fig 2.5 show that differential conductance be plotted in a larger bias-voltage range than those in Fig 2.4. In Fig 2.5, there are two $\partial I/\partial V$ lines intercept the conductance gap at V=35 meV. The quantized energy(35 meV) is arising from the internal vibrational modes. This structure correspond to the phenomenon that $C_{60}$ adsorb an energy about 35 meV and excited from the sphere mode to the prolate ellipsoid mode as shown in the inset of the Fig 2.3.

Thanks to these experimental results. They show the evidence that it is more and more possible that to study the effect of single molecule in the electronic transport.

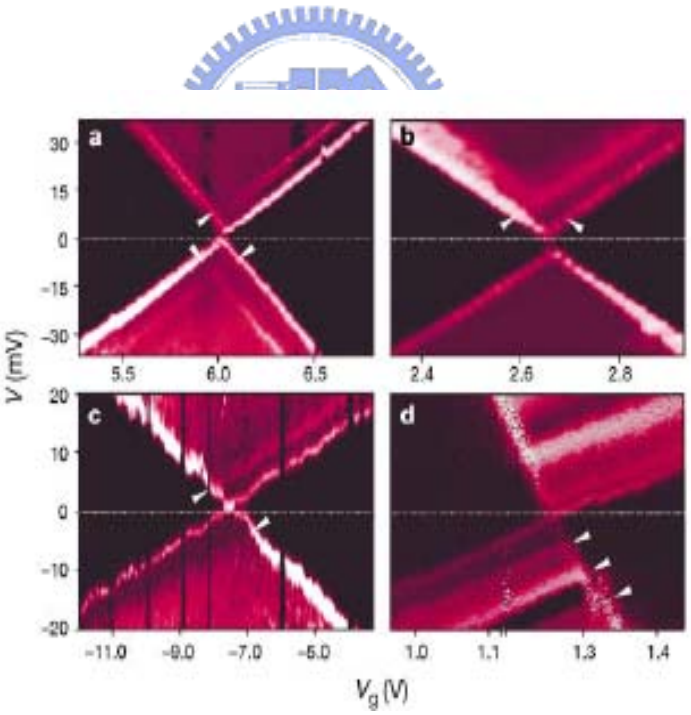


Fig 2.4 Experimental results extracted from H. Park. *et al.*[5].

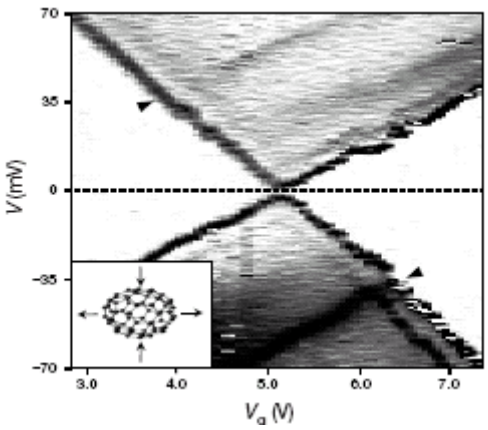


Fig 2.5 Experimental results extracted from H. Park. *et al*.[5].

# Chapter 3

# Landauer-Büttiker Formalism and Scattering Matrix Method

## 3.1 Introduction to the Landauer-Büttiker formalism

In this section, we introduce the multichannel Landauer-Büttiker formula starting from the single channel case. Full reference is available on the original paper of Büttiker et. a*l*. [21].

We assume that there are two reservoir of electrochemical potential $\mu_1$ and $\mu_2$ respectively connected by a 1D channel and there is a barrier in between the reservoirs.It is straightforward to calculate the current of this system if we assume that the contacts are "reflectionless", that is , the electrons can enter both side reservoirs from the 1D channel without suffering reflections. Numerical calculation indicate that as long as the energy is not too close to the bottom of band, an electron from1D channel into reservoirs can exit negligible probability reflection [22] .

Now, at zero temperature, we add a small bias at the two reservoirs. Because the contacts are "reflectionless", both side of electrons from reservoir 1 to 2 or reservoir 2 to 1 cancel out each other. So, only the transmitted electrons between $\mu_1$ and $\mu_2$ have distribution to the current from reservoir 1 to 2 . By the way, in 1D , J=I and the electron transfer the barrier with probability T.

By the definition, $I = -\rho \upsilon e$ where , $\rho = 2\frac{dn}{dE}(\mu_1 - \mu_2)T$ . In addition, $\frac{dn}{dE}(\mu_1 - \mu_2)T$ is the number of states per unit length that are injected from

reservior1 to reservior2 , 2 is spin factor ; $\upsilon = \frac{p}{m} = \frac{\hbar k_f}{m}$ .

Therefore, I can be written as

$$I = -2\frac{dn}{dE}(\mu_1 - \mu_2)T\frac{\hbar k_f}{m}$$

And at 1D,

$$\frac{dn}{dE} = \frac{dn}{dk}\frac{dk}{dE} = \frac{dk}{(2\pi/L)}\frac{1}{(\hbar^2 k_f/2m)} \quad \text{so}$$

$$G = \frac{I}{V} = \frac{I}{-e(\mu_1 - \mu_2)} = \frac{2e^2}{h}T$$

For the case of multichannel system, we assume there are $N \times N$ multi-channels with transmission electrons injected from reservior1 with channel n and propagating to reservior2 with channel m.

Therefore, the total transmission probability injected from channel n is then given by

$$T_n = \sum_{m=1}^{N} T_{nm}$$

Correspondingly the total current is $\sum_{n=1}^{N} I_n = \sum_{n=1}^{N}\sum_{m=1}^{N} T_{nm}$, and

total conductance $G = \sum_{n=1}^{N}\sum_{m=1}^{N}\frac{2e^2}{h}T_{nm}$

# 3.2 The Scattering Matrix Method

In this section we will employ scattering matrix method to our calculations. The scattering matrix which we now present as an alternative couples explicitly the outgoing states to the incoming states of a system. Here, we consider a N-layer multilayer structure, as shown in Fig. 3.1 .

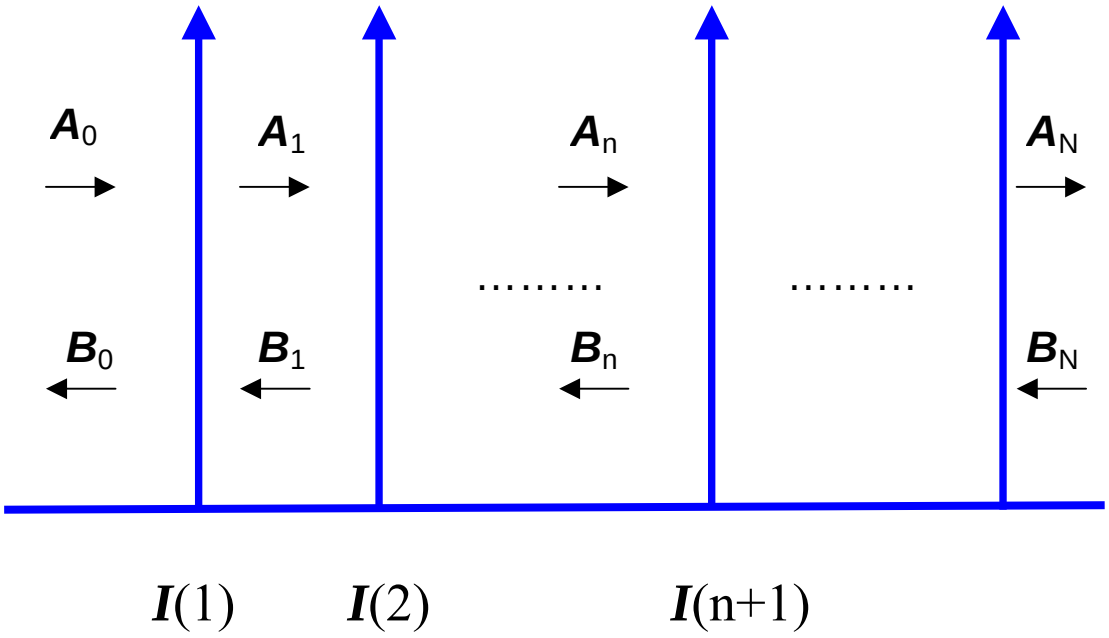


Fig. 3.1 A N-layer multilayer structure

$$\begin{bmatrix} \boldsymbol{A}_N \\ \boldsymbol{B}_0 \end{bmatrix} = \boldsymbol{S}(0,N)\begin{bmatrix} \boldsymbol{A}_0 \\ \boldsymbol{B}_N \end{bmatrix} \tag{3.1}$$

The coefficients $\boldsymbol{A}_N$ ,$\boldsymbol{B}_0$ of outgoing states are related to the coefficients $\boldsymbol{A}_0$ and $B_N$ of the incoming states via scattering matrix $\boldsymbol{S}(0,N)$.

For the nth-piece , we can define

$$\begin{bmatrix} \boldsymbol{A}_{n+1} \\ \boldsymbol{B}_n \end{bmatrix} = \boldsymbol{S}(n,n+1)\begin{bmatrix} \boldsymbol{A}_n \\ \boldsymbol{B}_{n+1} \end{bmatrix} \tag{3.2}$$

Moreover , we can get

$$\begin{bmatrix} \boldsymbol{A}_{n+1} \\ \boldsymbol{B}_{n+1} \end{bmatrix} = \boldsymbol{I}(n+1)\begin{bmatrix} \boldsymbol{A}_n \\ \boldsymbol{B}_n \end{bmatrix} \tag{3.3}$$

where $\boldsymbol{I}(n+1)$ is the interfacial matrix representing the coupling of the barrier and the eigenstates of the (n+1)th interface.

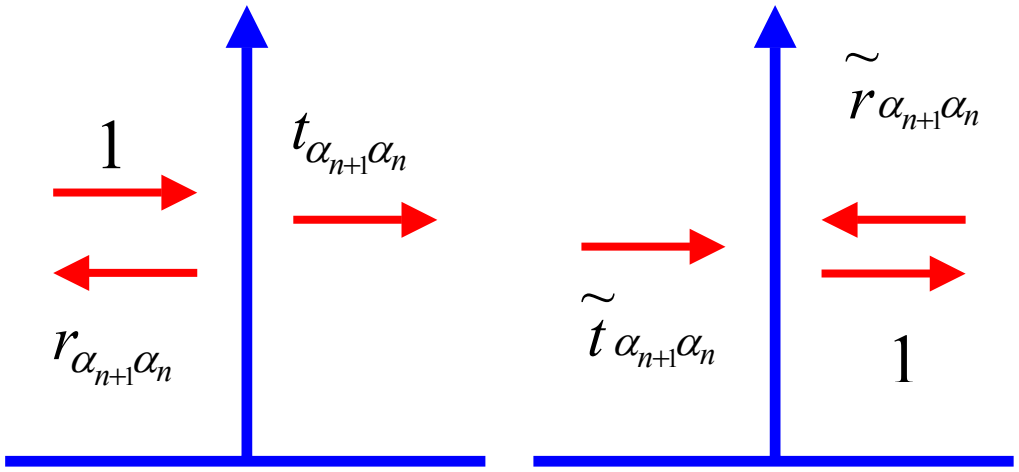


Fig. 3.2 The transmission and reflection coefficient incident from right or left hand side

$$\boldsymbol{S}(n,n+1)=\begin{bmatrix} t_{\alpha_{n+1}\alpha_n} & \tilde{r}_{\alpha_{n+1}\beta_{n+1}} \\ r_{\beta_j\alpha_j} & \tilde{t}_{\beta_n\beta_{n+1}} \end{bmatrix} \tag{3.4}$$

where $\alpha$ and $\beta$ are eigenstate index ; t and r are respectively transmission and reflection coefficient when electron incoming from left side ; $\tilde{t}$ and $\tilde{r}$ are transmission and reflection coefficient when electron incoming from right side

Easily , ***I***(n+1) can be represented as

$$\boldsymbol{I}(n+1)=\begin{bmatrix} t^{-1}{}_{\alpha_j\alpha_{j+1}} & -t^{-1}{}_{\alpha_j\alpha_{j+1}}\tilde{r}_{\alpha_{j+1}\beta_{j+1}} \\ r_{\beta_j\alpha_j}t^{-1}{}_{\alpha_j\alpha_{j+1}} & \tilde{t}_{\beta_j\beta_{j+1}}-r_{\beta_j\alpha_j}t^{-1}{}_{\alpha_j\alpha_j}\tilde{r}_{\alpha_{j+1}\beta_{j+1}} \end{bmatrix} \tag{3.5}$$

First , we start from calculate the two piece case as an example:

$$\begin{bmatrix} \boldsymbol{A}_1 \\ \boldsymbol{B}_0 \end{bmatrix}=\boldsymbol{S}(0,1)\begin{bmatrix} \boldsymbol{A}_0 \\ \boldsymbol{B}_1 \end{bmatrix} \tag{3.6}$$

where

$$\boldsymbol{S}(0,1)=\begin{bmatrix} t_{\alpha_1\alpha_0} & \tilde{r}_{\alpha_1\beta_1} \\ r_{\beta_0\alpha_0} & \tilde{t}_{\beta_0\beta_1} \end{bmatrix} \tag{3.7}$$

$$\begin{bmatrix} \boldsymbol{A}_1 \\ \boldsymbol{B}_1 \end{bmatrix} = \boldsymbol{I}(2)\begin{bmatrix} \boldsymbol{A}_2 \\ \boldsymbol{B}_2 \end{bmatrix} \tag{3.8}$$

where

$$\boldsymbol{I}(2)=\begin{bmatrix} t^{-1}{}_{\alpha_1\alpha_2} & -t^{-1}{}_{\alpha_1\alpha_1}\tilde{r}_{\alpha_2\beta_2} \\ r_{\beta_1\alpha_1}t^{-1}{}_{\alpha_1\alpha_2} & \tilde{t}_{\beta_j\beta_{j+1}} - r_{\beta_1\alpha_1}t^{-1}{}_{\alpha_1\alpha_2}\tilde{r}_{\alpha_2\beta_2} \end{bmatrix} \tag{3.9}$$

Eliminating $\boldsymbol{A}_1$ ,$\boldsymbol{B}_1$ , we have

$$\begin{bmatrix} \boldsymbol{A}_2 \\ \boldsymbol{B}_0 \end{bmatrix} = \boldsymbol{S}(0,2)\begin{bmatrix} \boldsymbol{A}_0 \\ \boldsymbol{B}_2 \end{bmatrix} \tag{3.10}$$

$$\boldsymbol{S}_{11}(0,2)=\left[\boldsymbol{I}_{11}(2)-\boldsymbol{S}_{12}(0,1)\boldsymbol{I}_{21}(2)\right]^{-1}\boldsymbol{S}(0,1)$$
$$\boldsymbol{S}_{12}(0,2)=\left[\boldsymbol{I}_{11}(2)-\boldsymbol{S}_{12}(0,1)\boldsymbol{I}_{21}(2)\right]^{-1}\left[\boldsymbol{S}_{12}(0,1)\boldsymbol{I}_{22}(2)-\boldsymbol{I}_{12}(2)\right]$$
$$\boldsymbol{S}_{21}(0,2)=\boldsymbol{S}_{21}(0,1)+\boldsymbol{S}_{22}(0,1)\boldsymbol{I}_{21}(2)\boldsymbol{S}_{11}(0,2)$$
$$\boldsymbol{S}_{22}(0,2)=\boldsymbol{S}_{22}(0,1)\boldsymbol{I}_{22}(2)+\boldsymbol{S}_{22}(0,1)\boldsymbol{I}_{21}(2)\boldsymbol{S}_{12}(0,2)$$

Similarly, the successive scattering matrixs $\boldsymbol{S}(0,3)$,$\boldsymbol{S}(0,2)$…….$\boldsymbol{S}(0,N)$ can be calculated , from which the final transmission and reflection coefficients of N-layer multiplayer structures can then be obtained using Eq. 3.1. Finally, we study a problem shown in appendix A to establish an independent check on our scattering matrix method.

# Chapter 4

# Local Phonon Effect On The Quantum Transport In a 1D Wire

## 4.1 Introduction

In this chapter, we make a complete and detailed analysis with a non-perturbed method on the quantum transport in a 1-D wire with interaction with a center-mass-oscillation local phonons. In the beginning, we show the model and formulation of local phonon in a 1-D wire. Next, we present the numerical results which including the electron-local phonon interaction strength $V$, mass of local phonon $M$, and phonon temperature ……etc dependence. As expected, the phonon sideband effects are small. And we try to enhance it in Ch. 5.

## 4.2 Model of Local Phonon in a 1D Wire

As shown in Fig. 4.1, we consider a single electron model, in which the electron propagates in a quasi-one dimensional system while interacting with a center-mass-oscillation impurity. The system under investigation can be described by the Hamiltonian ::

$$H_0 = -\frac{\hbar^2}{2m}\frac{\partial^2}{\partial x^2} - \frac{\hbar^2}{2M}\frac{\partial^2}{\partial y^2} + \frac{1}{2}M\omega^2 y^2 + V\delta(x-y) \qquad (4.1)$$

$x$ :: *electron propagating direction*

$y$ :: *impurity oscillation direction*

Here, ω denotes the frequency of phonon and Vδ(x-y) describes the interaction between the electron and local phonon.

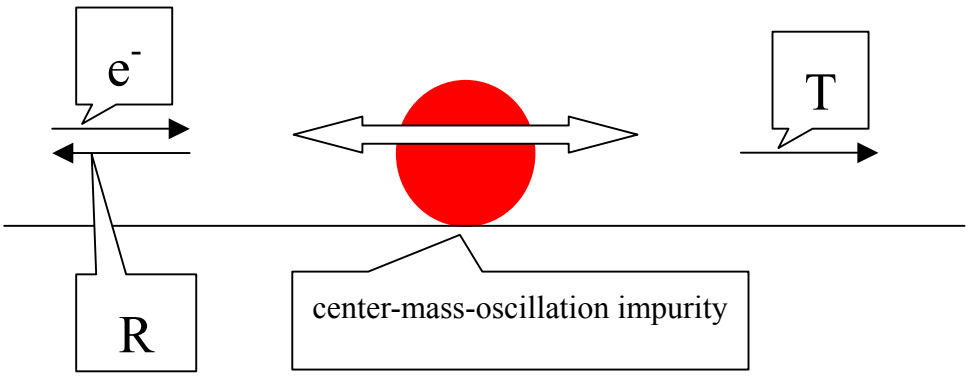


Fig. 4.1 The model of electron propagates in a quasi-one dimensional system while interacting with a center-mass-oscillation impurity

# 4.2 Formulation of Local Phonon in a 1D Wire

Here, we write down the formulation of the problem in section 4.1. It's dimensionless Hamiltonian can be written as:

$$H_D = -\frac{\partial^2}{\partial x^2} - \tilde{M}\frac{\partial^2}{\partial y^2} + \omega^2 y^2 + v\delta(x-y)\,, \qquad (4.2)$$

*where* $\tilde{M} = \frac{m}{M}$.

The energy unit is taken to be $E^* = \frac{\hbar^2 k_F^{\,2}}{2m^*}$, and length unit is $a^* = 1/k_F$, phonon frequency unit $\omega^* = \omega\hbar k_f^{\,2}\sqrt{1/mM}$, the unit of the strength of interaction $V^* = E^*/k_F$ and for GaAs $m^* = 0.067m_e$.

Mathematically, we can write $V\delta$ (x-y)= $\sum_i V\delta(x-x_i)\delta(y-y_i)dx$ ,which is represented by a series of delta-function potential. This allows us to solve the problem via scattering matrix method.

Before we construct the scattering matrix, we need a complete basis to expand the wave function. To proceed, we start from the basis wave function obeying the equation:

$$H_y\Phi_n(y)=\left(-\tilde{M}\frac{\partial^2}{\partial y^2}+\omega^2 y^2\right)\Phi_n(y)=E_n\Phi_n(y). \tag{4.3}$$

Assuming y= $\alpha\ \xi$ , with $\alpha=\left(\tilde{M}/\omega^2\right)^{1/4}$ ,

we can get

$$H_\xi\Phi_n(\xi)=\left(-\frac{\partial^2}{\partial\xi^2}+\omega^2\xi^2\right)\Phi_n(\xi)=E_n\Phi_n(\xi)\ . \tag{4.4}$$

where $E_n=(2n+1)\omega_p, \omega_p=\left(\tilde{M}\omega^2\right)^{1/2}$

$$\Phi_n(\xi)=\frac{1}{\sqrt{2^n n!}}\left(\frac{1}{\pi}\right)^{1/2}\mathrm{Exp}\left(-\frac{\xi^2}{2}\right)H_n(\xi)\ , \tag{4.5}$$

and $H_n(\xi)$ is Hermite function.

With the complete basis, we can write down the form of wave function at the neighbors of x=$x_j$ as shown in Fig. 4. 2 and try to construct the $\mathcal{S}$(j, j+1) matrix.

For an electron incident from phonon sideband n=$n_0$, the scattering wave function would be of the form.

$$\begin{cases}\Psi(x,\xi)=\sum_{n=0}^{\infty}\delta_{nn_0}e^{ik_n x}\Phi_n(\xi)+\sum_{n=0}^{\infty}r_{nn_0}e^{-ik_n x}\Phi_n(\xi)\text{.....in the regionI}\\ \Psi(x,y)=\sum_{n=0}^{\infty}t_{nn_0}e^{ik_n x}\Phi_n(y)\text{.....in the regionII}\end{cases} \tag{4.6}$$

where n is the phonon mode index , and $k_m = \sqrt{\varepsilon - (2n+1)\omega_p}$ is the wave vector of an electron, where $\varepsilon$ is the total energy of the system including the propagating electron and total phonons.

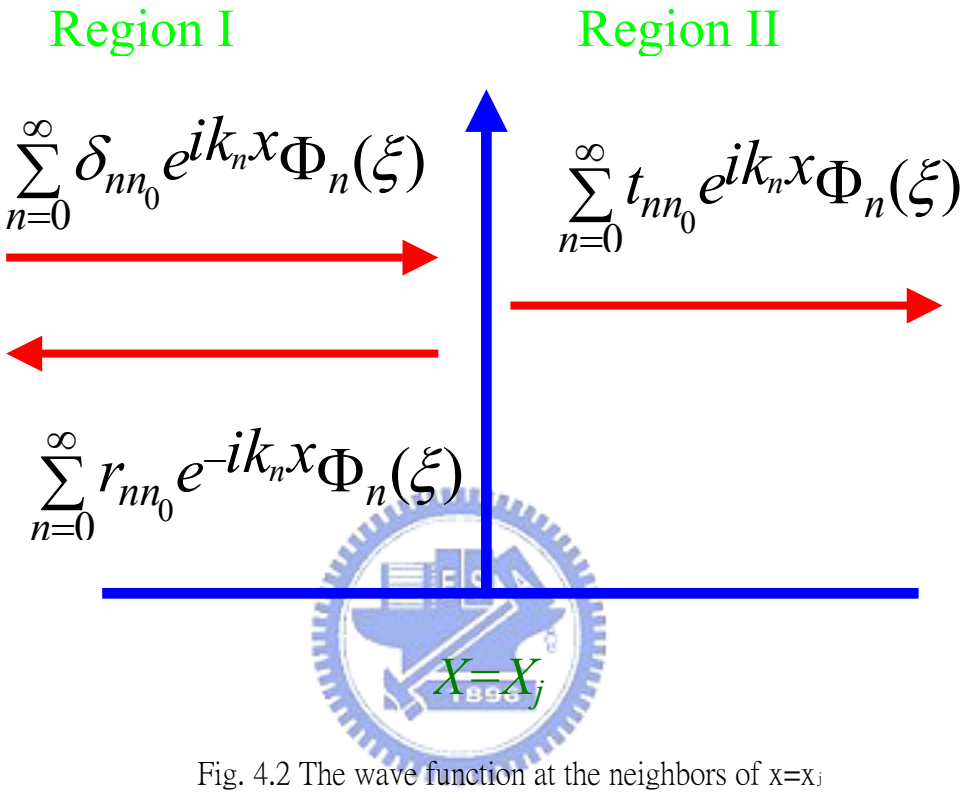


Fig. 4.2 The wave function at the neighbors of $x=x_j$

Performing the matching of the boundary condition at $x=x_j$ , as follows:

wave function continuous at $x=x_j$ , we get

$$\sum_{n=0}^{\infty} \delta_{nn_0} e^{ik_n x_j} \Phi_n(\xi) + \sum_{n=0}^{\infty} r_{nn_0} e^{-ik_n x_j} \Phi_n(\xi) = \sum_{n=0}^{\infty} t_{nn_0} e^{ik_n x_j} \Phi_n(\xi). \tag{4.7}$$

Multiplying Eq. 4.7 by $\int_{-\infty}^{\infty} \Phi_{n'}(\xi) d\xi$ , we have

$$\sum_{n=0}^{\infty} \delta_{nn_0} e^{ik_n x_j} \int_{-\infty}^{\infty} \Phi_{n'}(\xi)\Phi_n(\xi) d\xi + \sum_{n=0}^{\infty} r_{nn_0} e^{-ik_n x_j} \int_{-\infty}^{\infty} \Phi_{n'}(\xi)\Phi_n(\xi) d\xi \tag{4.8}$$

$$= \sum_{n=0}^{\infty} t_{nn_0} e^{ik_n x_j} \int_{-\infty}^{\infty} \Phi_{n'}(\xi)\Phi_n(\xi) d\xi.$$

Matching the derivative of the wave function at $x=x_j$ we get

$$\sum_{n=0}^{\infty} ik_n \delta_{nn_0} e^{ik_n x_j} \Phi_n(\xi) + \sum_{n=0}^{\infty} (-ik_n) r_{nn_0} e^{-ik_n x_j} \Phi_n(\xi)$$
$$-\sum_{n=0}^{\infty} (ik_n) t_{nn_0} e^{ik_n x_j} \Phi_n(\xi) + \frac{Vdx}{\alpha} \delta(\xi - x_j/\alpha) \sum_{n=0}^{\infty} t_{nn_0} e^{ik_n x_j} \Phi_n(\xi) \quad (4.9)$$
$$= 0.$$

Multiplying Eq. 4.9 by $\int_{-\infty}^{\infty} \Phi_{n'}(\xi) d\xi$, we have

$$\sum_{n=0}^{\infty} ik_n \delta_{nn_0} e^{ik_n x_j} \int_{-\infty}^{\infty} \Phi_{n'}(\xi)\Phi_n(\xi) d\xi + \sum_{n=0}^{\infty} (-ik_n) r_{nn_0} e^{-ik_n x_j} \int_{-\infty}^{\infty} \Phi_{n'}(\xi)\Phi_n(\xi) d\xi$$
$$-\sum_{n=0}^{\infty} (ik_n) t_{nn_0} e^{ik_n x_j} \int_{-\infty}^{\infty} \Phi_{n'}(\xi)\Phi_n(\xi) d\xi + \frac{Vdx}{\alpha} \sum_{n=0}^{\infty} t_{nn_0} e^{ik_n x_j} \int_{-\infty}^{\infty} \Phi_{n'}(\xi)\Phi_n(\xi) \delta(\xi - x_j/\alpha) d\xi$$
$$= 0 . \quad (4.10)$$

Rewrite Eq (4.8) and Eq (4.10), we can construct the following matrix equation:

$$\begin{bmatrix} \boldsymbol{M}_{11} & \boldsymbol{M}_{12} \\ \boldsymbol{M}_{21} & \boldsymbol{M}_{22} \end{bmatrix} \begin{bmatrix} \boldsymbol{r}_{nn_0} \\ \boldsymbol{t}_{nn_0} \end{bmatrix} = \begin{bmatrix} \boldsymbol{c}_1 \\ \boldsymbol{c}_2 \end{bmatrix} \quad (4.11)$$

Here, submatrixs are given by

$$\boldsymbol{M}_{11} = e^{-ik_n x_j} \delta_{n'n} \quad (4.12)$$
$$\boldsymbol{M}_{12} = -e^{ik_n x_j} \delta_{n'n}$$
$$\boldsymbol{M}_{21} = -ik_n e^{-ik_n x_j} \delta_{n'n}$$
$$\boldsymbol{M}_{22} = \frac{Vdx}{\alpha} e^{ik_n x_j} \Phi_{n'}\left(\xi/\alpha\right) \Phi_n\left(\xi/\alpha\right) - ik_n e^{ik_n x_j} \delta_{n'n}$$

$$(\boldsymbol{C}_1)_{n'} = -e^{ik_n x_j} \delta_{n'n_0} \quad (4.13)$$
$$(\boldsymbol{C}_2)_{n'} = -ik_{n_0} e^{ik_n x_j} \delta_{n'n_0}$$

Solving Eg. 4.11 we can obtain the column $\boldsymbol{r}_{n_0}$ and $\boldsymbol{t}_{n_0}$. Similarly, if we let electron incident from n=1,n=2……..n=M, we can get the $M \times M$ matrix of $r_{\alpha\beta}$ and $t_{\alpha\beta}$ ,where $\alpha$ , $\beta$ are phonon mode index.

Subsequently, in the similar way, we also get the $M \times M$ matrix of $\tilde{\boldsymbol{r}}_{\alpha\beta}$ and $\tilde{\boldsymbol{t}}_{\alpha\beta}$. Therefore, we can construct the **S**(j, j+1) matrix from Eq. 3.7, which is written as :

$$\boldsymbol{S}(j,j+1)=\begin{bmatrix} \boldsymbol{t}_{\alpha_{j+1}\alpha_j} & \tilde{\boldsymbol{r}}_{\alpha_{j+1}\beta_{j+1}} \\ \boldsymbol{r}_{\beta_j\alpha_j} & \tilde{\boldsymbol{t}}_{\beta_n\beta_{j+1}} \end{bmatrix} \tag{4.14}$$

Using Eq. 3.10, we can get the matrix $\boldsymbol{S}(0, 2)$. Similarly, the successive scattering matrixs $\boldsymbol{S}(0,3)$,S(0,2)…….$\boldsymbol{S}(0,N)$ can be calculated and $\boldsymbol{S}(0,N)$ is written as

$$\boldsymbol{S}_{11}(0,N)=\left[\boldsymbol{I}_{11}(N)-\boldsymbol{S}_{12}(0,N-1)\boldsymbol{I}_{21}(N)\right]^{-1}\boldsymbol{S}(0,N-1)$$
$$\boldsymbol{S}_{12}(0,N)=\left[\boldsymbol{I}_{11}(N)-\boldsymbol{S}_{12}(0,N-1)\boldsymbol{I}_{21}(N)\right]^{-1}\left[\boldsymbol{S}_{12}(0,N-1)\boldsymbol{I}_{22}(N)-\boldsymbol{I}_{12}(N)\right]$$
$$\boldsymbol{S}_{21}(0,N)=\boldsymbol{S}_{21}(0,N-1)+\boldsymbol{S}_{22}(0,N-1)\boldsymbol{I}_{21}(N)\boldsymbol{S}_{11}(0,N)$$
$$\boldsymbol{S}_{22}(0,N)=\boldsymbol{S}_{22}(0,N-1)\boldsymbol{I}_{22}(N)+\boldsymbol{S}_{22}(0,N-1)\boldsymbol{I}_{21}(2)\boldsymbol{S}_{12}(0,N)$$

From Eq. 3.10 let column $\boldsymbol{A}_0=\delta_{nn_0}$ and $\boldsymbol{B}_N$=0, then

$$\mathrm{T}=\sum_{n_0}\sum_{m'}\frac{k(m')}{k(n_0)}\left(\left|t_{m'n_0}\right|\right)^2P(n_0)$$
$$R=\sum_{n_0}\sum_{m'}\frac{k(m')}{k(n_0)}\left(\left|r_{m'n_0}\right|\right)^2P(n_0)$$
$$G=\frac{2e^2}{h}\mathrm{T}$$

where $P(n_0)=(1-e^{-\beta\hbar\omega})e^{-\beta n\hbar\omega}$, $\beta$ =$\mathrm{K_BT}$, $\mathrm{K_B}$ is the Boltzmann constant and T is absolute temperature.

# 4.3 Numerical Result and Discussion

In this section, we show the numerical results and discussions of the local phonon effect on the quantum transport in a 1-D wire in several different cases. In all of cases, we study the G characteristics as a function of incident electron energy at zero phonon temperature except in the case considering the dependence of phonon temperature. Therefore, we take the G with units $2e^2/h$ as the vertical axis and the energy of incident energy called E as the horizontal axis.

## The dependence of electron-local phonon interaction strength V

In Fig. 4.3, we take the frequency of local phonon $\omega$=1.83 THz, the mass of

phonon $M$=20m$^*$, the phonon energy $\hbar\omega$=1.2meV as energy scale, and interaction strength V varying from -0.2 to -0.8 with units $7.12\times10^{-11}$ eV • m. In these cases of attractive local phonon potential, we can see two interesting phenomena. First, dip structures appear near the energy with $\hbar\omega$. This is because that the system will have a quasi-bound state near the phonon sideband bottom. Therefore, we can find that the position of the dip is directly proportion to the $1/V^2$. Second, from the dip structures, it is found that as the interaction strengths $V$ become stronger, dip structures become wider, which cause the incident electron has shorter life time staying in the quasi-bound state

In Fig. 4.4, we take the frequency of local phonon ω=1.83 THz, mass of phonon $M$=20m$^*$, the phonon energy ħω as energy scale equal to1.2 mev , and interaction strength $V$ varying from 0.2 to 0.8 with units $7.12\times10^{-11}$ eV • m. In these cases of repulsive local phonon potentials, no dip structures are found in G. Only the kinks happen near each phonon's sideband structure. However, as the energy of incident electron increase, the kinks disappear and the transmission coefficient throughout the effective delta potential approach to unity.

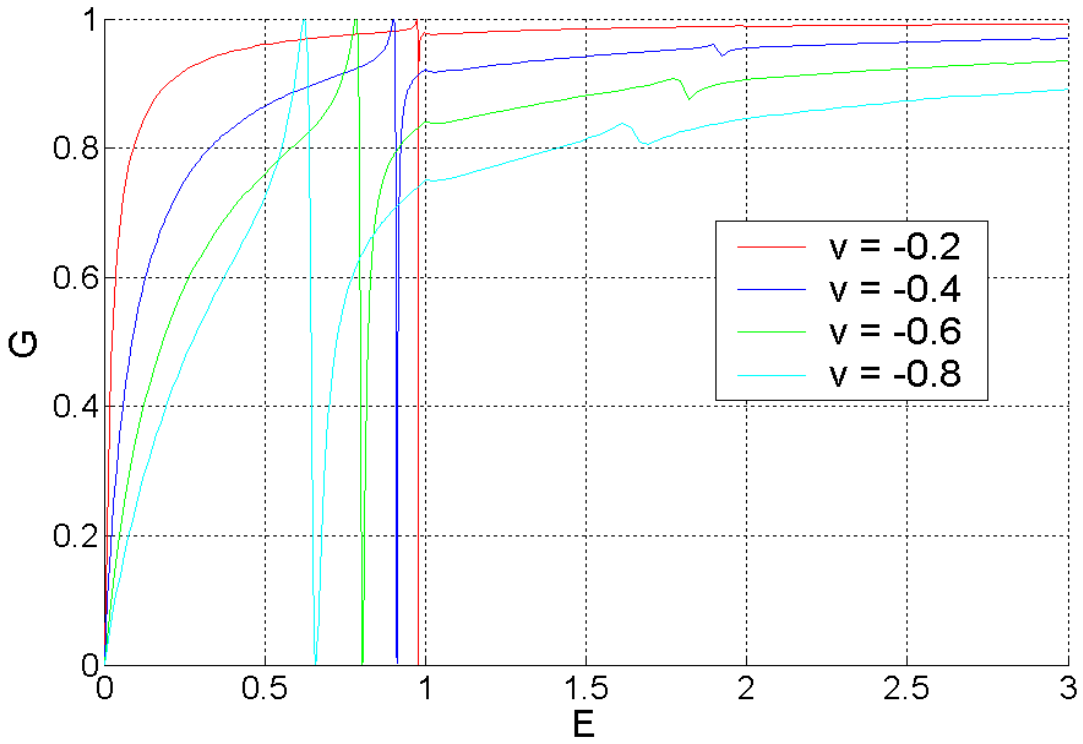


Fig 4.3: G with unit $2e^2/h$ plotted against energy of incident electron with unit $\hbar\omega$ = 1.2meV for ω = 1.83THz, zero phonon temperature, and mass of phonon $M = 20m^*$ for attractive local phonon potentials' strength $V$ varying from -0.2 to -0.8 with units $7.12\times10^{-11}$ eV • m.

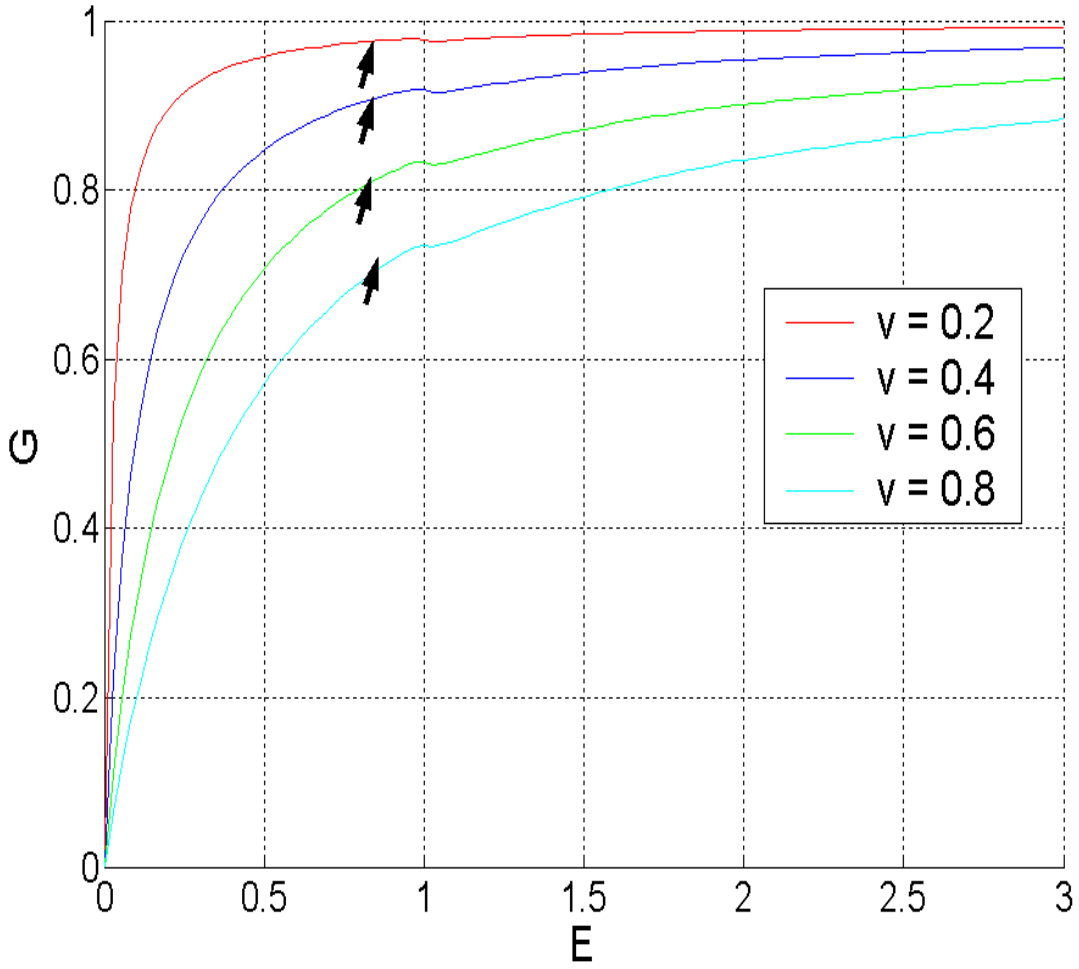


Fig. 4.4: G with unit $2e^2/h$ plotted against energy of incident electron with unit $\hbar\omega$ = 1.2meV for $\omega$ = 1.83THz, zero phonon temperature, and mass of phonon $M$ = 20m$^*$ for attractive local phonon potentials' strength $V$ varying from 0.2 to 0.8 with units $7.12\times10^{-11}$ eV • m.

## The dependence of the local phonon's frequency

In Fig. 4.5, we take the oscillation frequency of local phonon ωvarying from 1.83 to 7.32. THz, mass of phonon $M$=20m$^*$, the $E_f$ =9meV as energy scale, and interaction strength $V$= 0.6 with units $7.12\times10^{-11}$ eV • m to repulsive local phonon potential. In this case, it is found that the phonon sideband structures become weak when the local phonon oscillation frequency increase, which can explain by the classical formula $\omega$ =

($k/M$) where k is string constant. As the oscillation frequency is higher, the string constant $k$ also become larger causing the hardness for the electron to interact with the phonon., which resulting sideband structures become weaker.

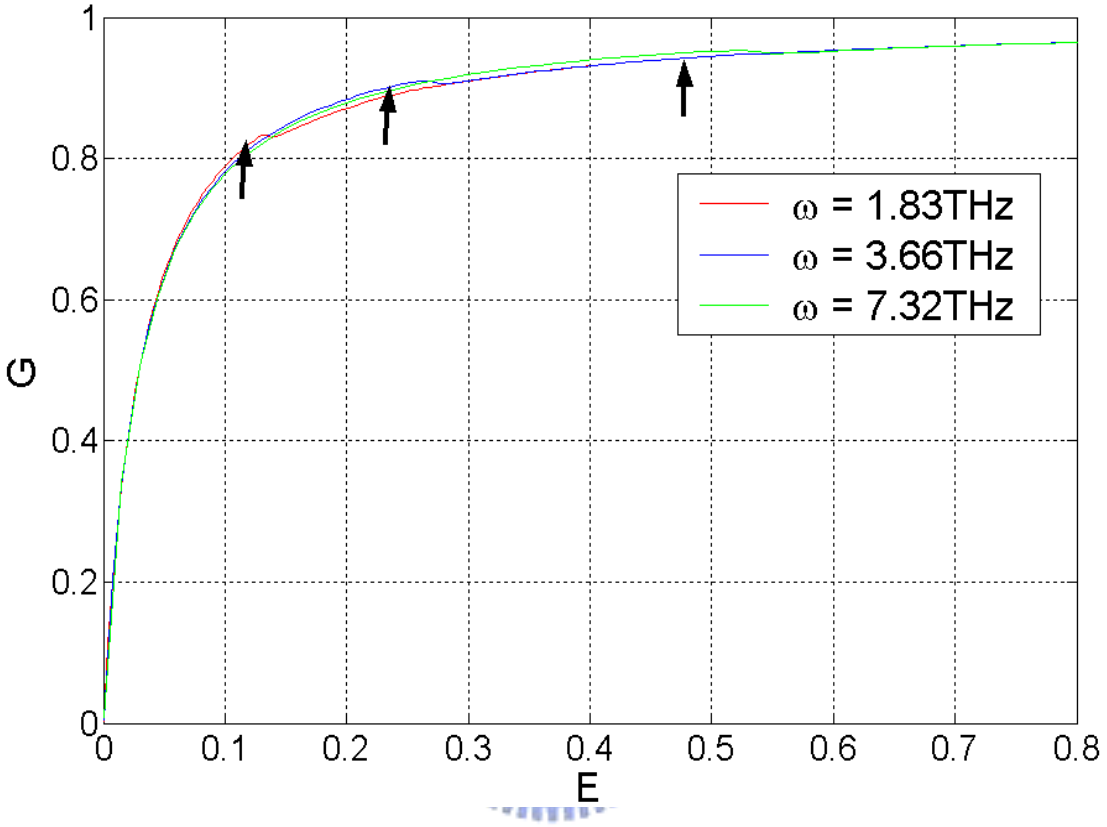


Fig. 4.5: G with unit $2e^2/h$ plotted against energy of incident electron with unit $E_F$ =9meV for $V$= 0.6 with units $7.12\times10^{-11}$ eV • m to repulsive local potential, zero phonon temperature and mass of phonon $M$ = 20m$^*$ for various frequencies of local phonon.

## The dependence of the local phonon's oscillation mode when the electron incident

In Fig. 4.6 and 4.7, we take the oscillation frequency of local phonon $\omega$ = 1.83 THz, mass of phonon $M$=20m$^*$, the phonon energy $\hbar\omega$=1.2meV as energy scale, and interaction strength $V$ = 0.6 and -0.6 with units $7.12\times10^{-11}$ev/m respectively to repulsive and attractive potential. In Fig. 4.6 and 4.7, the different curves show the

cases in which of different numbers of phonon modes n. In Fig. 4.6 and 4.7, the effect of phonon sideband structure become stronger as the local phonon staying in higher mode n, the hardness of electron–local phonons interaction is reduced due the higher energy of local phonons. Therefore, we can see the fruitful structures. In Fig. 4.8, we take the oscillation frequency of local phonon $\omega = 1.83$ THz, mass of phonon $M$=20m$^*$, the phonon energy $\hbar\omega$=1.2mev as energy scale, interaction strength $V = 0.6$ with units $7.12\times10^{-11}$ eV • m respectively to repulsive potential, and the number of phonon number n = 10 while the electron incident. We can find that $T_{10->10}$+ $T_{10->11->10}$+ $T_{10->9->10}$ dominate the total transmission.

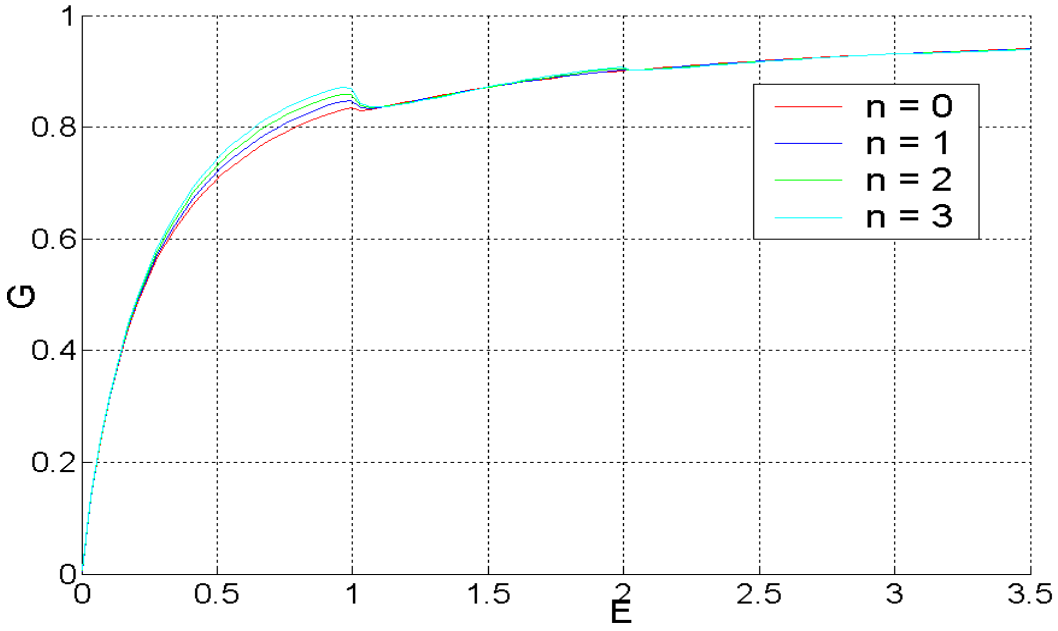


Fig. 4.6: G with unit $2e^2/h$ plotted against energy of incident electron with unit $\hbar\omega$ = 1.2meV for $\omega$ = 1.83THz, zero phonon temperature, and mass of phonon $M$ = 20m$^*$, and for attractive local phonon potentials' strength $V$ = -0.6 with units $7.12\times10^{-11}$ eV • m with various numbers of phonon mode n.

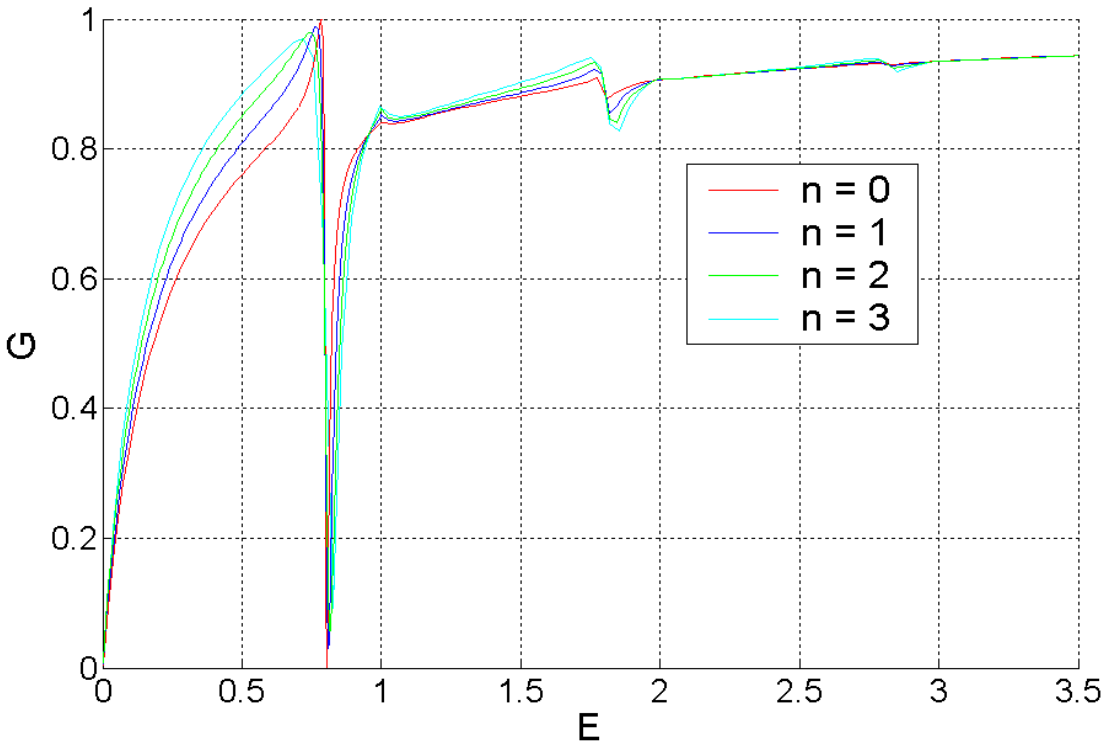


Fig. 4.7: G with unit $2e^2/h$ plotted against energy of incident electron with unit $\hbar\omega$ = 1.2meV for $\omega$ = 1.83THz, zero phonon temperature, and mass of phonon $M = 20m^*$, and for attractive local phonon potentials' strength $V$ = -0.6 with units $7.12\times10^{-11}$ eV • m with various numbers of phonon mode n.

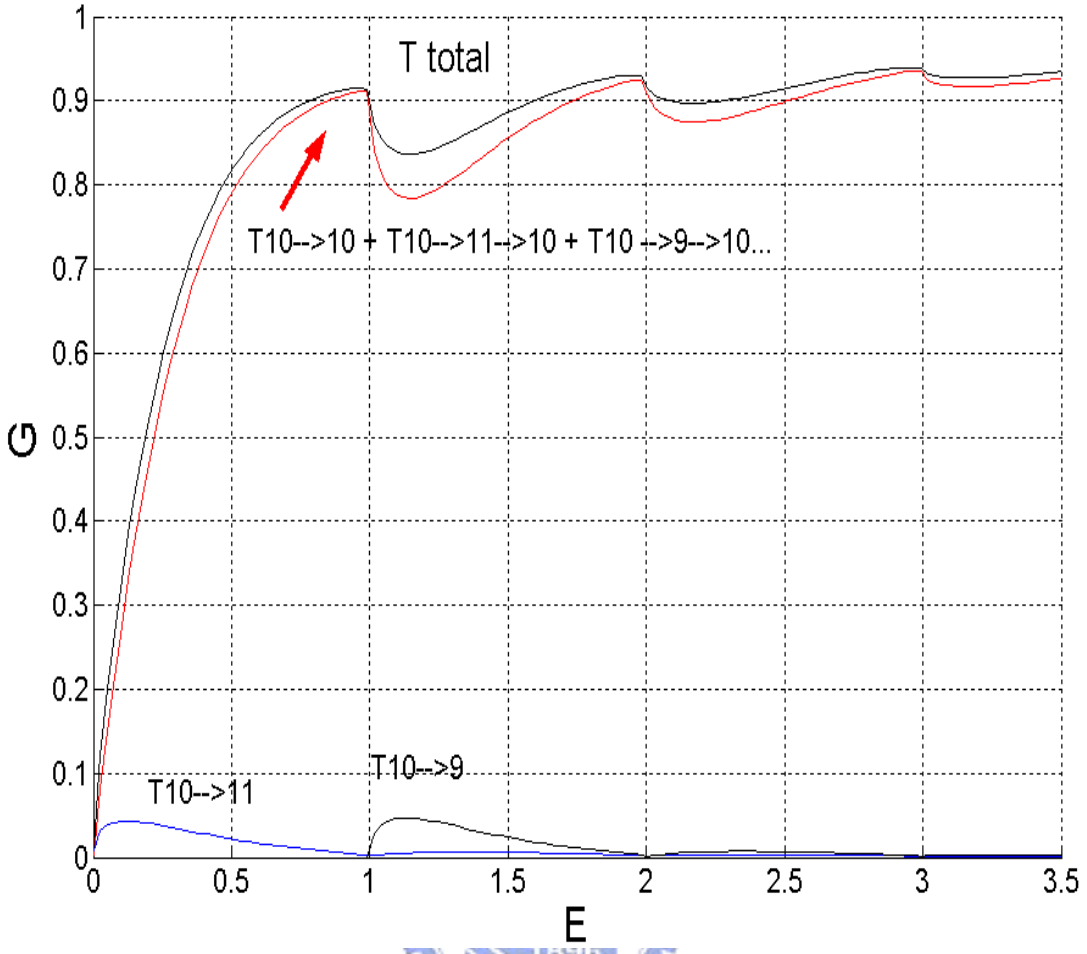


Fig 4.8: T plotted against energy of incident electron with unit ħω = 1.2meV for ω = 1.83THz, repulsive local phonon potentials' strength V = 0.6 with units $7.12\times10^{-11}$ eV • m, and the number of phonon mode n = 10 while the electron incident. Black line corresponds to $T_{total.}$ Red line corresponds to $T_{10->10}$+ $T_{10->11->10}$+ $T_{10->9->10}$. Blue line corresponds to $T_{10->11.}$ Green line correspond to $T_{10->9.}$

## The dependence of phonon temperature

In Fig. 4.9, we take the oscillation frequency of local phonon $\omega = 1.83$ THz, mass of phonon $M$=20m$^*$, the phonon energy $\hbar\omega$=1.2meV as energy scale, and interaction strength V = 0.6 with units $7.12\times10^{-11}$ eV • m respectively to repulsive and attractive potential and $k_BT$ varying from 0 to 5 ħω. Although the phonon sideband

structures become larger as local phonons mode n increase. The sideband structures would be smeared by thermal averageing. In addition, as increasing temperature, the local phonons have higher energy, which has more ability to interact with the electron. Therefore, the conductance is harder to saturate to unity in high energy regime.

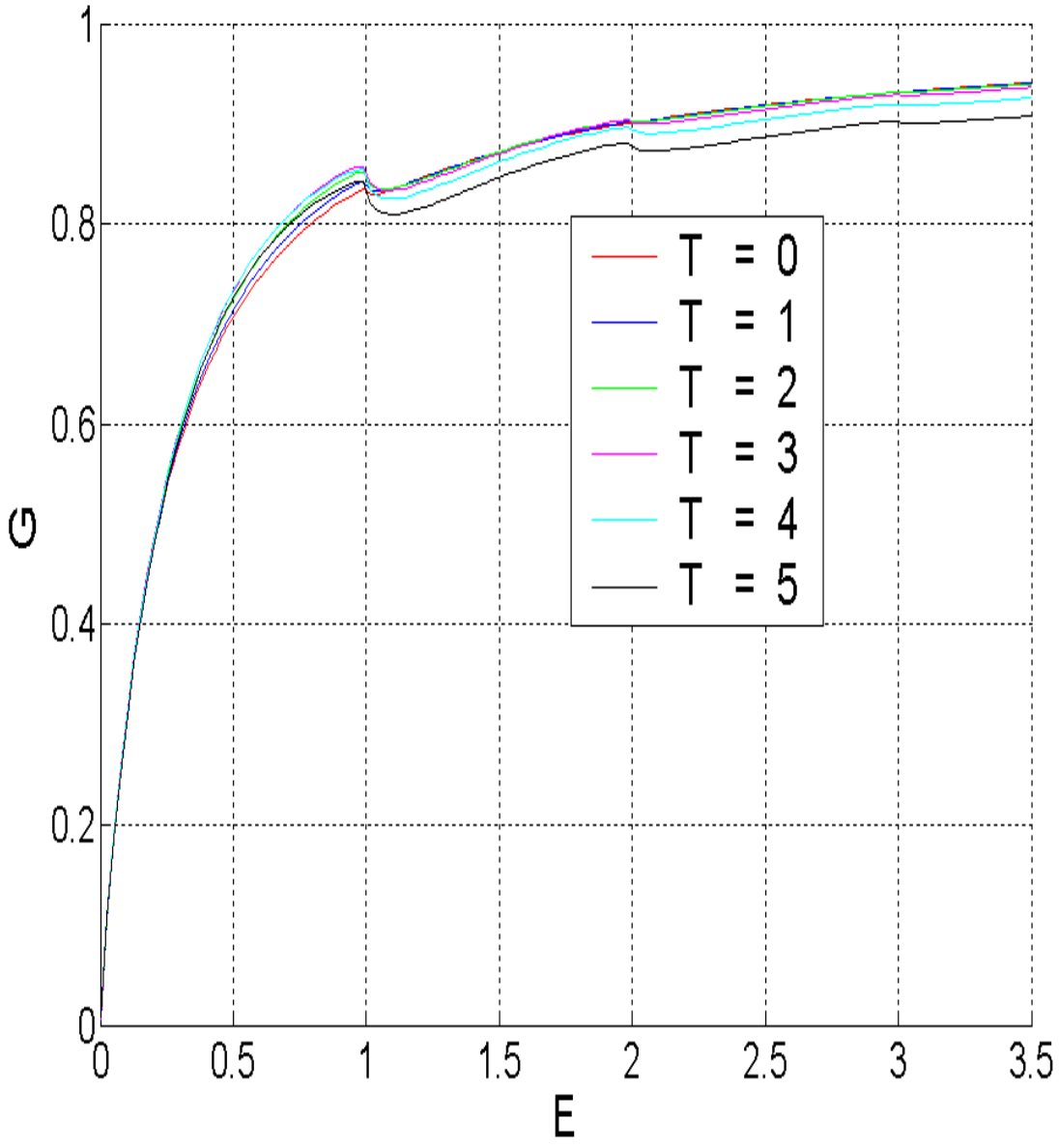


Fig. 4.9: G with unit $2e^2/h$ plotted against energy of incident electron with unit $\hbar\omega$ = 1.2meV for $\omega$ = 1.83THz, zero phonon temperature, and mass of phonon $M = 20m^*$, and for repulsive local phonon potentials' strength $V = 0.6$ with units $7.12\times10^{-11}$ eV • m with various phonon temperature 0 to 5 $T$ with unit $K_b/\hbar\omega$.

## The local phonon mass dependence

In Fig. 4.10 and 4.11, we take the oscillation frequency of local phonon $\omega = 1.83$ THz, , the phonon energy $\hbar\omega = 1.2$meV as energy scale, and interaction strength $V =$ 0.6 and -0.6 with units $7.12 \times 10^{-11}$ eV・m , mass of phonon $M$ varying from 20 to 80 $m^*$ and 20 to 1000 $m^*$ respectively for repulsive and attractive potential. In Fig. 4.10, we can find the phonon sideband structure will disappear as the phonon's mass increasing to 100 $m^*$ in the repulsive case. It is because the oscillation phonon is harder to interact with electron when it's mass is heavier. We can also realize it from the local phonon's wave function. As the local phonon mass increases, its wave function becomes more localized. Therefore, the electron-phonon interaction barrier become more and like a single repulsive delta function barrier and the sideband structure will disappear gradually. However, for the attractive case, we can see that the dip structure in attractive case even the mass of local phonon increases to 100 $m^*$. This is because that even though the electron-phonon attractive interaction barrier turns to like static single attractive delta function, it can make the quasi-bound state causing dip structure.

In summary, in this section, we have discussed the electron transport through local phonons in a 1-D channel, including the effect of interaction strength V, oscillation frequency $\omega$ ,phonon temperature $T_{ph}$, and mass of oscillation impurity M.

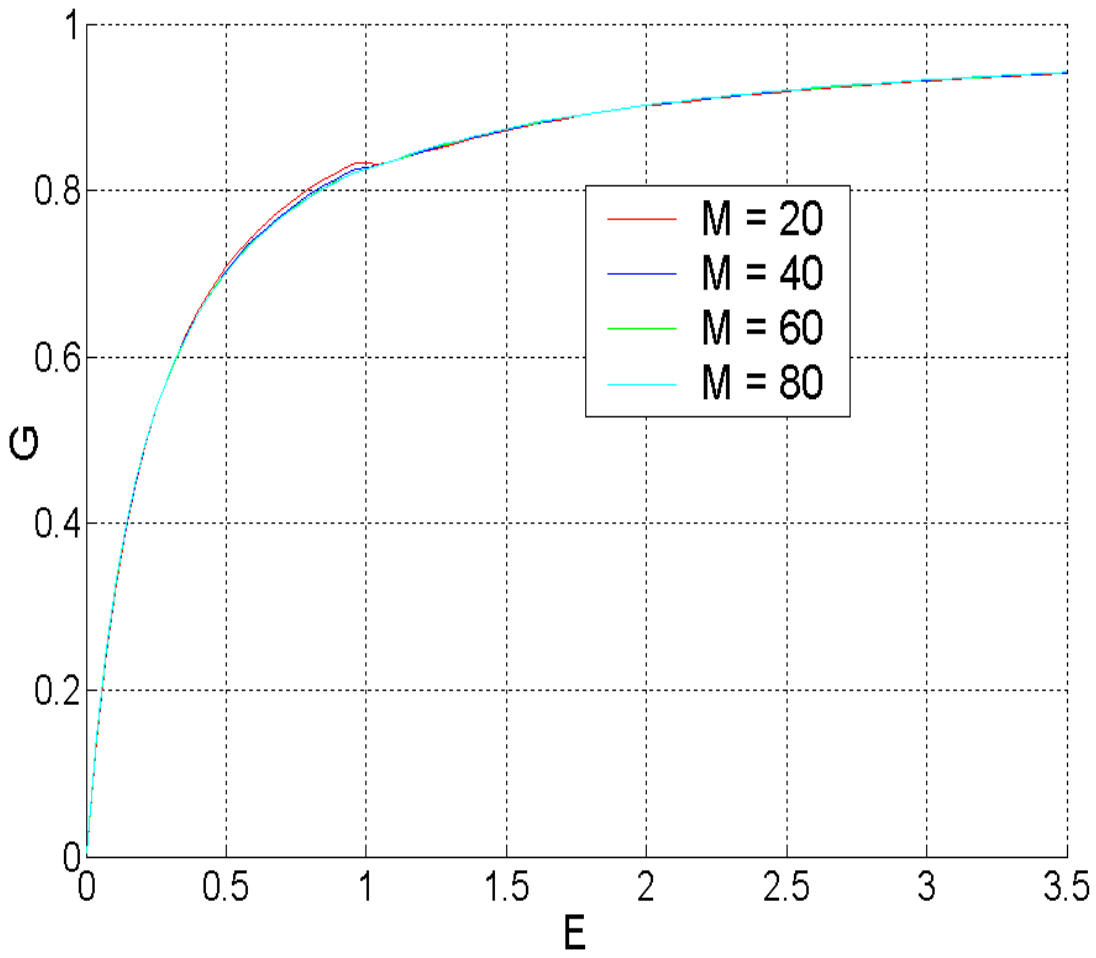


Fig. 4.10: G with unit $2e^2/h$ plotted against energy of incident electron with unit $\hbar\omega$ = 1.2meV for $\omega$ = 1.83THz, zero phonon temperature, and for repulsive local phonon potentials' strength $V$ = 0.6 with units $7.12\times10^{-11}$ eV・m with mass of phonon M varying from $20m^*$ to $80m^*$.

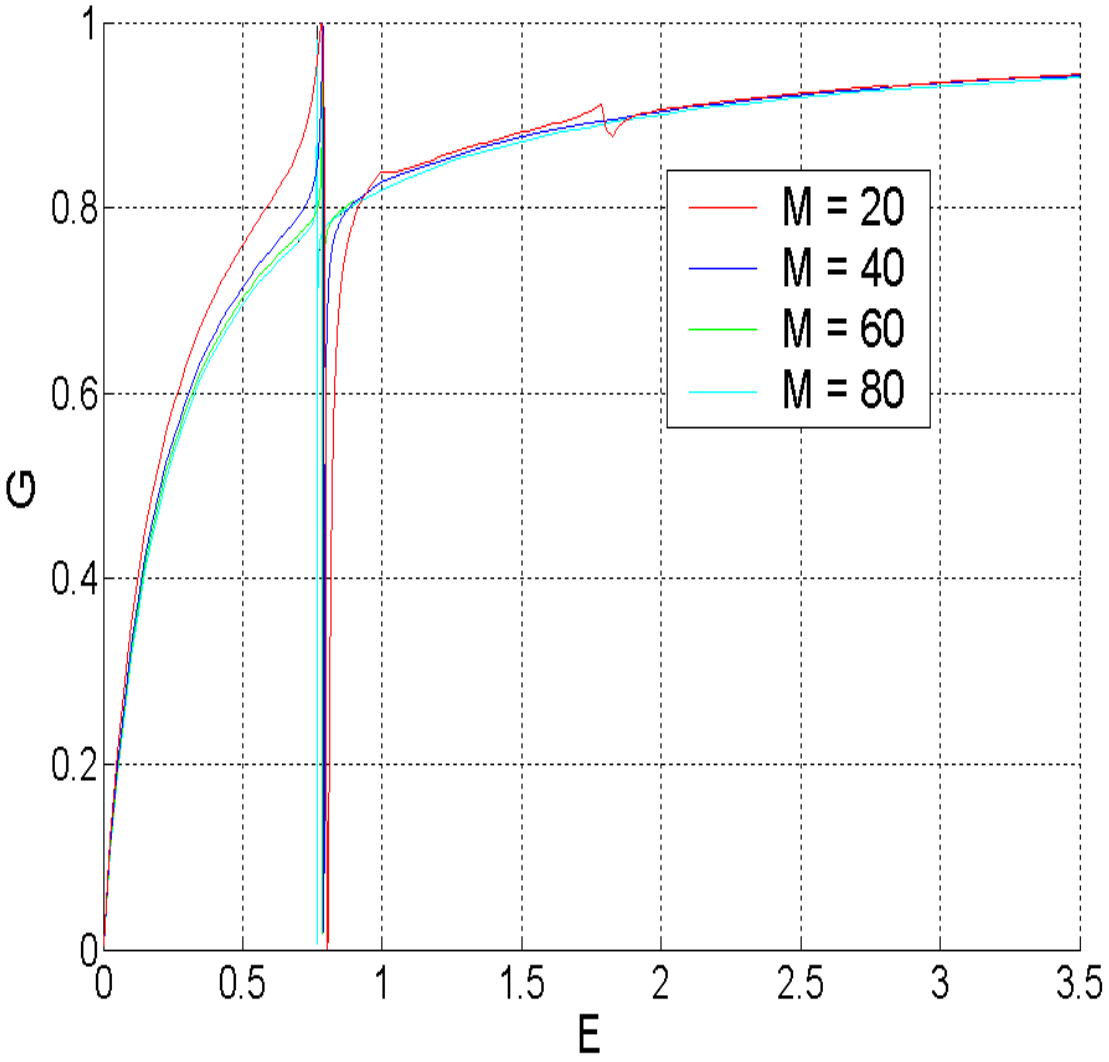


Fig. 4.11: G with unit $2e^2/h$ plotted against energy of incident electron with unit $\hbar\omega$ = 1.2meV for $\omega$ = 1.83THz, zero phonon temperature, and for attractive local phonon potentials' strength $V$ = -0.6 with units $7.12\times10^{-11}$ eV • m with mass of phonon M varying from $20m^*$ to $80m^*$.

# Chapter 5

# Local Phonon Effect In a Quantum Dot On The Quantum Transport

## 5.1 Introduction

In order to describe the experimental results about $C_{60}$ center-mass-oscillation in single-molecular device worked by H. Park. *et al.*[5]. In this chapter, we take the analyses made in Ch. 4 as basis to study the electron tunneling through the single-molecular quantum dot embedded with center-mass-oscillation local phonons. First, we show the model and formulation. Next, we present our numerical results and discussions. And our numerical shows that, in addition to the main peaks related to tunneling through the dot, the phonon sideband peaks due to electron-local phonons interaction appear. Moreover, we can enhance this effect by shortening the width of the dot to reduce the wavelength of electron.

## 5.2 Model of the electron resonant tunneling through a quantum dot coupled with local phonons

In Fig. 5.1, we consider a single electron model, in which the electron propagates from a 1D wire into a quantum dot while interacting with a local phonon staying in the quantum dot. The system under investigation can be described by the Hamiltonian,

$$H = H_0 + V\delta(x-y) + V_{DB}$$

where $H_0$ is shown in Eq. 4.1 and $V_{DB}$ represents the double barrier modeling the

quantum dot is written as

$V_{DB} = V_0\delta(x+L_2)+V_0\delta(x-L_2)$

where $V_0$ is related to the strength of the double barrier and $2L_2$ is the width of the quantum dot.

## 5.3 Formulation of Local Phonon in a Quantum Dot

In this section, we derive the formula of Local Phonon Effect In a Quantum Dot On The Quantum Transport which calculation is quietly similar to that in section 4.2.

We can also write down the dimensionless Hamiltonian as

$H_{DD} = H_D + \upsilon_0\delta(x+L_2)+\upsilon_0\delta(x-L_2)$

where we take the same units as shown in section 4.2

Here, we especially add two delta barrier $\upsilon_0\delta(x+L_2)+\upsilon_0\delta(x-L_2)$ outside the series delta-function potential arising from the $\upsilon\delta(x-y)$. Therefore we can also numerically solve this problem with scattering matrix method. Moreover, we can use the same basis as shown in Eg. 4.1.

Next, let's illustrate the process of constructing the scattering matrix **S(0, N)**. First, we need to matching at x = -L2 to get the scattering matrix **S(0, 1).** Seen in Fig. 5.2. For an electron incident from phonon sideband $n=n_0$ of region I , the scattering wave function would be of the form.

$$\begin{cases} \Psi(x,\xi) = \sum_{n=0}^{\infty}\delta_{nn_0}e^{ik_nx}\Phi_n(\xi)+\sum_{n=0}^{\infty}r_{nn_0}e^{-ik_nx}\Phi_n(\xi)\text{..... in the regionI} \\ \Psi(x,y) = \sum_{n=0}^{\infty}t_{nn_0}e^{ik_nx}\Phi_n(y)\text{.....in the regionII} \end{cases} \quad (5.1)$$

where n is the phonon sideband index , and $k_m = \sqrt{\varepsilon - (2n+1)\omega_p}$ ,where $\varepsilon$ is the total energy of the system including the propagating electron and the local system.

Performing the matching of the boundary condition at x=-L2.

Wavefunction continuous at x=-L2, matching at both sides, we get

$$\sum_{n=0}^{\infty} \delta_{nn_0} e^{ik_n(-L2)} \Phi_n(\xi) + \sum_{n=0}^{\infty} r_{nn_0} e^{-ik_n(-L2)} \Phi_n(\xi) = \sum_{n=0}^{\infty} t_{nn_0} e^{ik_n(-L2)} \Phi_n(\xi) \tag{5.2}$$

Multiplying Eq. 5. 2 by $\int_{-\infty}^{\infty} \Phi_{n'}(\xi) d\xi$ , we have

$$\sum_{n=0}^{\infty} \delta_{nn_0} e^{ik_n(-L_2)} \int_{-\infty}^{\infty} \Phi_{n'}(\xi) \Phi_n(\xi) d\xi + \sum_{n=0}^{\infty} r_{nn_0} e^{-ik_n(-L_2)} \int_{-\infty}^{\infty} \Phi_{n'}(\xi) \Phi_n(\xi) d\xi \tag{5.3}$$
$$= \sum_{n=0}^{\infty} t_{nn_0} e^{ik_n(-L_2)} \int_{-\infty}^{\infty} \Phi_{n'}(\xi) \Phi_n(\xi) d\xi$$

Matching the derivative of the wave function at x=-L2,, we get

$$\sum_{n=0}^{\infty} ik_n \delta_{nn_0} e^{ik_n(-L_2)} \Phi_n(\xi) + \sum_{n=0}^{\infty} \left(-ik_n\right) r_{nn_0} e^{-ik_n(-L_2)} \Phi_n(\xi)$$
$$-\sum_{n=0}^{\infty} \left(ik_n\right) t_{nn_0} e^{ik_n(-L_2)} \Phi_n(\xi) + V_0 \delta\left(\xi - (-L_2)/\alpha\right) \sum_{n=0}^{\infty} t_{nn_0} e^{ik_n(-L_2)} \Phi_n(\xi) \tag{5.4}$$
$$= 0$$

Multiplying Eq. 5. 4 by $\int_{-\infty}^{\infty} \Phi_{n'}(\xi) d\xi$ , we have

$$\sum_{n=0}^{\infty} ik_n \delta_{nn_0} e^{ik_n x_j} \int_{-\infty}^{\infty} \Phi_{n'}(\xi) \Phi_n(\xi) d\xi + \sum_{n=0}^{\infty} \left(-ik_n\right) r_{nn_0} e^{-ik_n x_j} \int_{-\infty}^{\infty} \Phi_{n'}(\xi) \Phi_n(\xi) d\xi$$
$$-\sum_{n=0}^{\infty} \left(ik_n\right) t_{nn_0} e^{ik_n x_j} \int_{-\infty}^{\infty} \Phi_{n'}(\xi) \Phi_n(\xi) d\xi + \frac{Vdx}{\alpha} \sum_{n=0}^{\infty} t_{nn_0} e^{ik_n x_j} \int_{-\infty}^{\infty} \Phi_{n'}(\xi) \Phi_n(\xi) \delta\left(\xi - x_j/\alpha\right) d\xi \tag{5.5}$$
$$= 0$$

Rewrite Eq. 5.3 and Eq. 5.5 in matrix form, we can construct the following matrix equation

$$\begin{bmatrix} \boldsymbol{N}_{11} & \boldsymbol{N}_{12} \\ \boldsymbol{N}_{21} & \boldsymbol{N}_{22} \end{bmatrix} \begin{bmatrix} \boldsymbol{r}_{nn_0} \\ \boldsymbol{t}_{nn_0} \end{bmatrix} = \begin{bmatrix} \boldsymbol{D}_1 \\ \boldsymbol{D}_2 \end{bmatrix} \tag{5.6}$$

Here, submatrixs are given by

$$\boldsymbol{N}_{11} = e^{-ik_n(-L_2)}\delta_{n'n}$$
$$\boldsymbol{N}_{12} = -e^{ik_n(-L_2)}\delta_{n'n}$$
$$\boldsymbol{N}_{21} = -ik_n e^{-ik_n(-L_2)}\delta_{n'n}$$
$$\boldsymbol{N}_{22} = V_0 e^{ik_n(-L_2)} - ik_n e^{ik_n(-L_2)}\delta_{n'n}$$

$$\left(\boldsymbol{D}_1\right)_{n'} = -e^{ik_n(-L_2)}\delta_{n'n_0}$$
$$\left(\boldsymbol{D}_2\right)_{n'} = -ik_{n_0} e^{ik_n(-L_2)}\delta_{n'n_0}$$

Solve Eq. 5.6 we can get the column $\boldsymbol{r}_{n_0}$ and $\boldsymbol{t}_{n_0}$. Similarly, if we let electron incident from n=1,n=2……..n=M, we can get the $M \times M$ matrix of $\boldsymbol{r}_{\alpha\beta}$ and $\boldsymbol{t}_{\alpha\beta}$, where $\alpha$, $\beta$ are phonon sideband index.

Subsequently, in the similar way, we also get the $M \times M$ matrix of $\tilde{\boldsymbol{r}}_{\alpha\beta}$ and $\tilde{\boldsymbol{t}}_{\alpha\beta}$. With matrix $\boldsymbol{r}_{\alpha\beta}$, $\boldsymbol{t}_{\alpha\beta}$, $\tilde{\boldsymbol{r}}_{\alpha\beta}$, and $\tilde{\boldsymbol{t}}_{\alpha\beta}$, we get scattering matrix **S**(0, 1) matrix by Eq. 3.7. In addition, we have constructed the **S**(1, 2),**S**(2, 3)…to **S**(N-2, N-1) matrix last chap. And, we construct the S(N-1, N) by the same way of constructing S(0, 1) matrix except replacing the $-L_2$ with $L_2$. With **S**(0, 1), **S**(1, 2)……..**S**(N-1, N) matrix. we can get the S(0,N) scattering matrix by scattering matrix method as mentioned in Section 3.2 finally.

Let column $\mathbf{A}_0 = \delta_{nn_0}$ and $\mathbf{B}_N = \mathbf{0}$. Then

$$T = \sum_{n_0}\sum_{m'} \frac{k(m')}{k(n_0)} \left(\left|t_{m'n_0}\right|\right)^2 P(n_0)$$
$$R = \sum_{n_0}\sum_{m'} \frac{k(m')}{k(n_0)} \left(\left|r_{m'n_0}\right|\right)^2 P(n_0)$$

$$G = \frac{2e^2}{h} T$$

where $P(n_0) = (1 - e^{-\beta\hbar\omega}) e^{-\beta n\hbar\omega}$, $\beta = K_B T$, $K_B$ is the Boltzmann constant and T is absolute temperature.

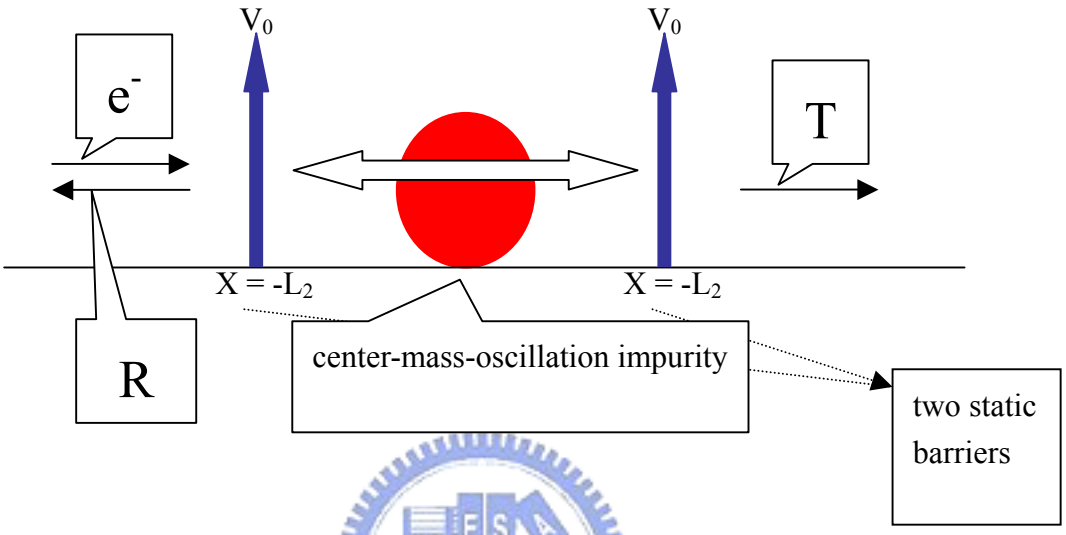


Fig. 5.1 Model of electron tunneling through a single-molecular quantum dot embedded with center-mass-oscillation local phonons

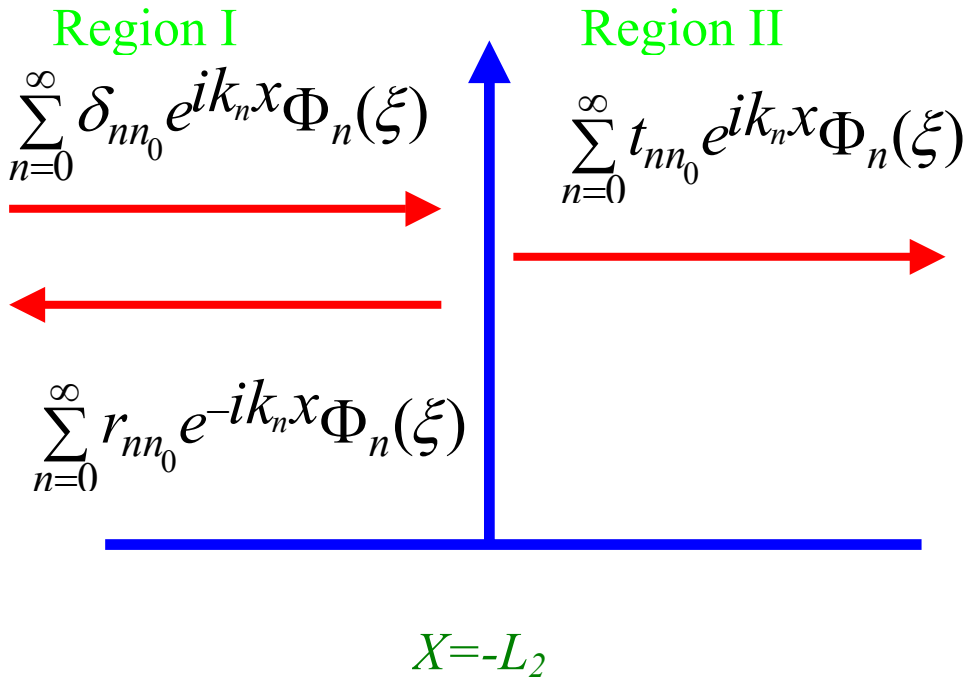


Fig. 5.2 The wave function at the neighbors of x=-L2

## 5.3 Numerical Result and Discussion

In this section, we show the numerical results and discussions of a electron tunneling through a quantum dot coupled with local phonons different cases. In all of cases, we study the G characteristics as a function of incident electron energy. Therefore, we take the G with units 2e/h as the vertical axis and the energy of incident energy called E as the horizontal axis

### The phonon sideband peaks

In Fig 5.3, the electron-local phonon interaction strengths vary from V=0.2 to 0.4 with units $7.12\times10^{-11}$ eV • m and we take the phonon energy ħω=0.12meV as energy scale, mass of phonon M=20m$^{*}$, and the strength of double barrier $V_0$ = 5 with unit $7.12\times10^{-11}$ eV • m at zero phonon temperature. In addition, the black line correspond to the conductance resulting from electron tunneling through the double barrier modeling the quantum dot. The separation between the phonon sidepeaks and the main resonance peak due to electron tunneling through the double barriers is about by the phonon energy ħω. The phonon sidepeaks are related to the excitation of local phonons by the electron tunneling onto the quantum dot. And at zero temperature, the electron tunneling onto the quantum dot can only excite phonons but absorb no phonon, which explain why the phonon sidepeaks only appear in right hand side of main resonance peaks.

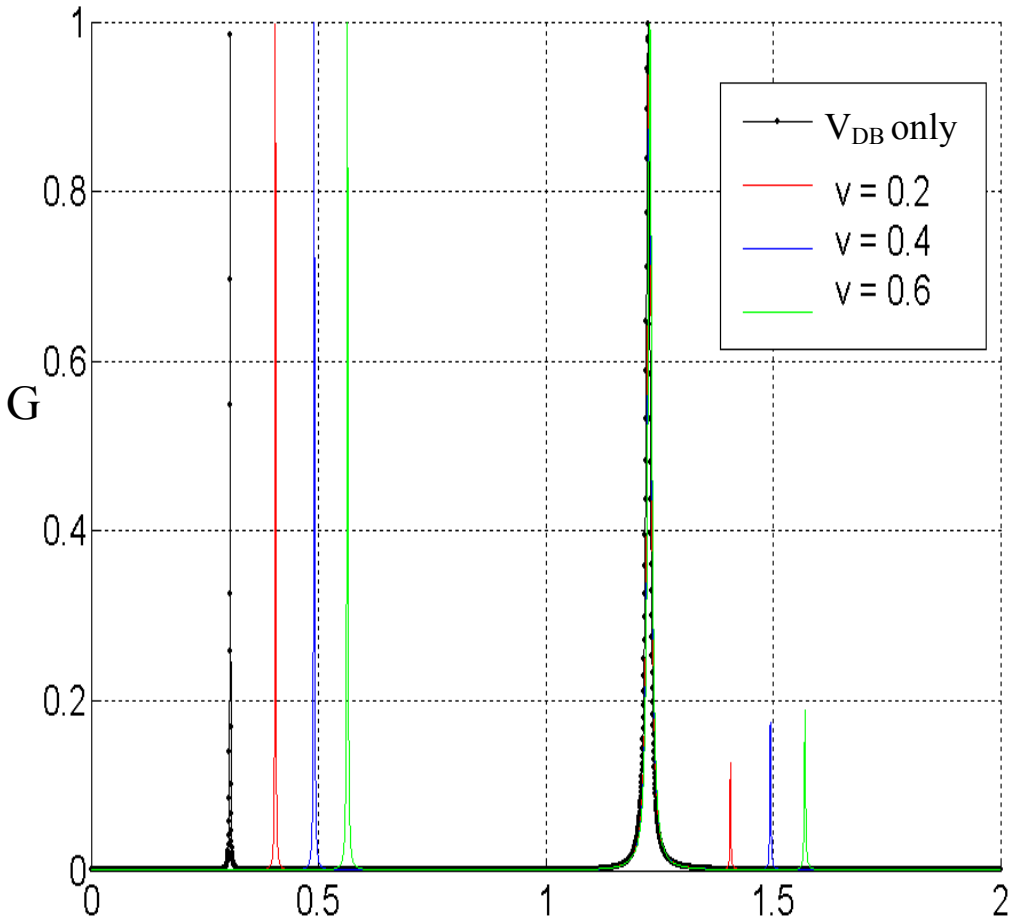


Fig 5.3: G with unit $2e^2/h$ plotted against energy of incident electron with unit $\hbar\omega$ = 1.2meV as energy scale for ω = 1.83THz, zero phonon temperature, and mass of phonon $M = 20m^*$ for repulsive local phonon potentials' strength $V$ varying from 0.2 to 0.6 with units $7.12 \times 10^{-11}$ eV • m.

## The incident electron wavelength dependence for repulsive local phonon potential at zero phonon temperature

In Fig 5.4, 5.5, 5.6 and 5.7, the widths of double barrier are respectively W=16, 20, 24,32 nm and we take the phonon energy ħω=2.14 with unit 9meV, mass of phonon M=1000m$^*$, the strength of double barrier $V_0$ =30 and electron-local phonon V= 30 with unit $7.12\times10^{-11}$ eV • m at zero phonon temperature. Those figures respectively shown in the inset of Fig 5.4 to 5.7 are the locally enlarged figures of phonon sidepeak. In this series of figures, we can find that the phonon sidepeaks can be enhanced 100 times height as the widths of double barrier become narrower from 16 nm to 32nm. It is because that the incident electron wave is confined in the double barrier. Therefore, as the width of double barrier is down to 16 .nm, the electron wavelength is also down to16 nm, which can be compared with the phonon wavelength at ground state about 1.6 nm and enhance the phonon sidepeaks.

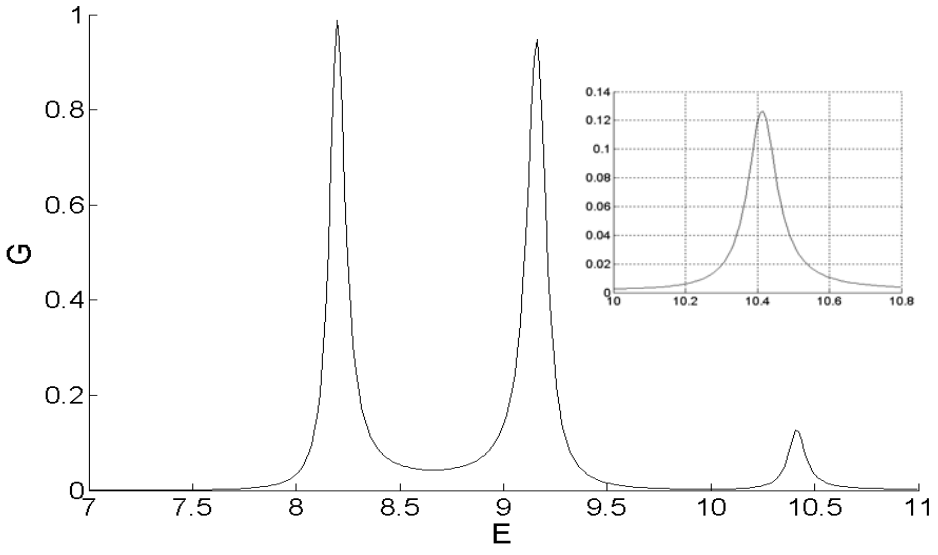


Fig. 5.4: G with unit $2e^2/h$ plotted against energy of incident electron with unit $E_F$ =9meV for $V$= 30 with units $7.12\times10^{-11}$ eV • m to repulsive local potential, zero phonon temperature, width of static barrier 16 nm, phonon energy $\hbar\omega$ = 19.2meV, and mass of phonon $M$ = 1000m$^*$.

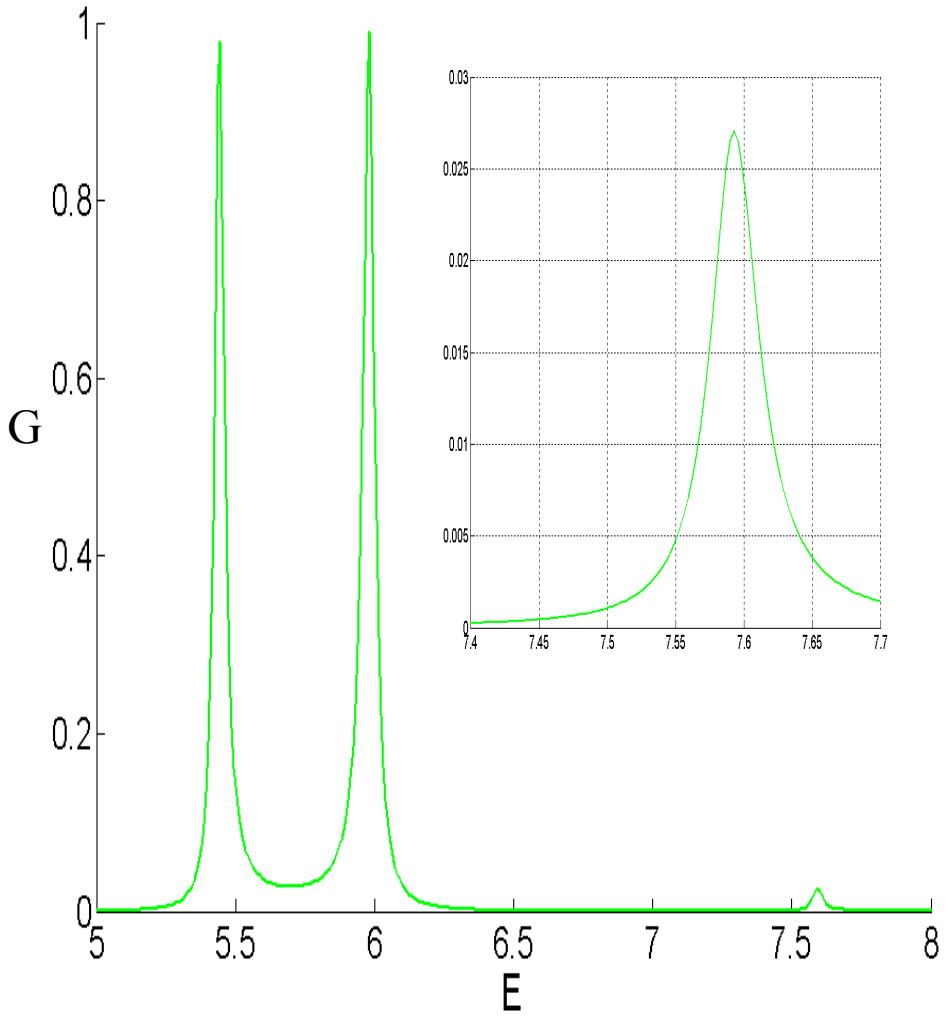


Fig. 5.5: G with unit $2e^2/h$ plotted against energy of incident electron with unit $E_F$ =9meV for $V$= 30 with units $7.12\times10^{-11}$ eV • m to repulsive local potential, zero phonon temperature, width of static barrier 20 nm, phonon energy $\hbar\omega$ = 19.2meV, and mass of phonon $M = 1000m^*$

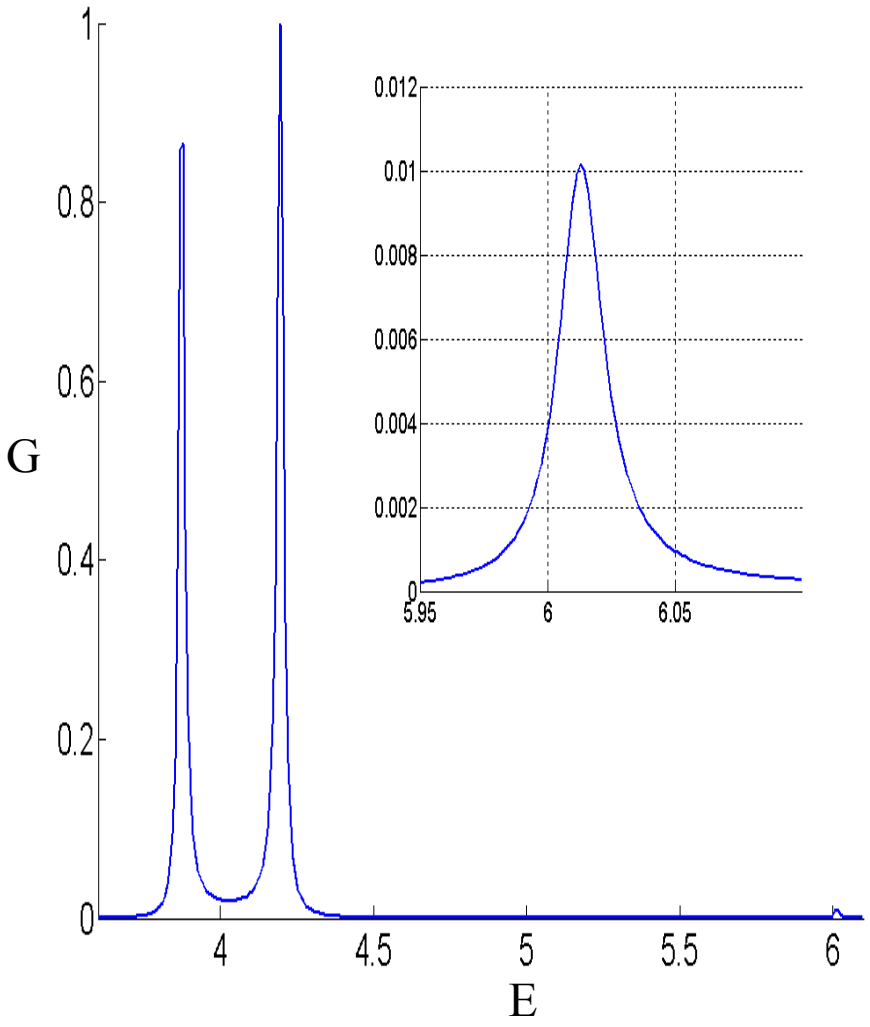


Fig. 5.6: G with unit $2e^2/h$ plotted against energy of incident electron with unit $E_F$ =9meV for $V$= 30 with units $7.12\times10^{-11}$ eV • m to repulsive local potential, zero phonon temperature, width of static barrier 24 nm, phonon energy $\hbar\omega$ = 19.2meV, and mass of phonon $M$ = 1000m$^*$

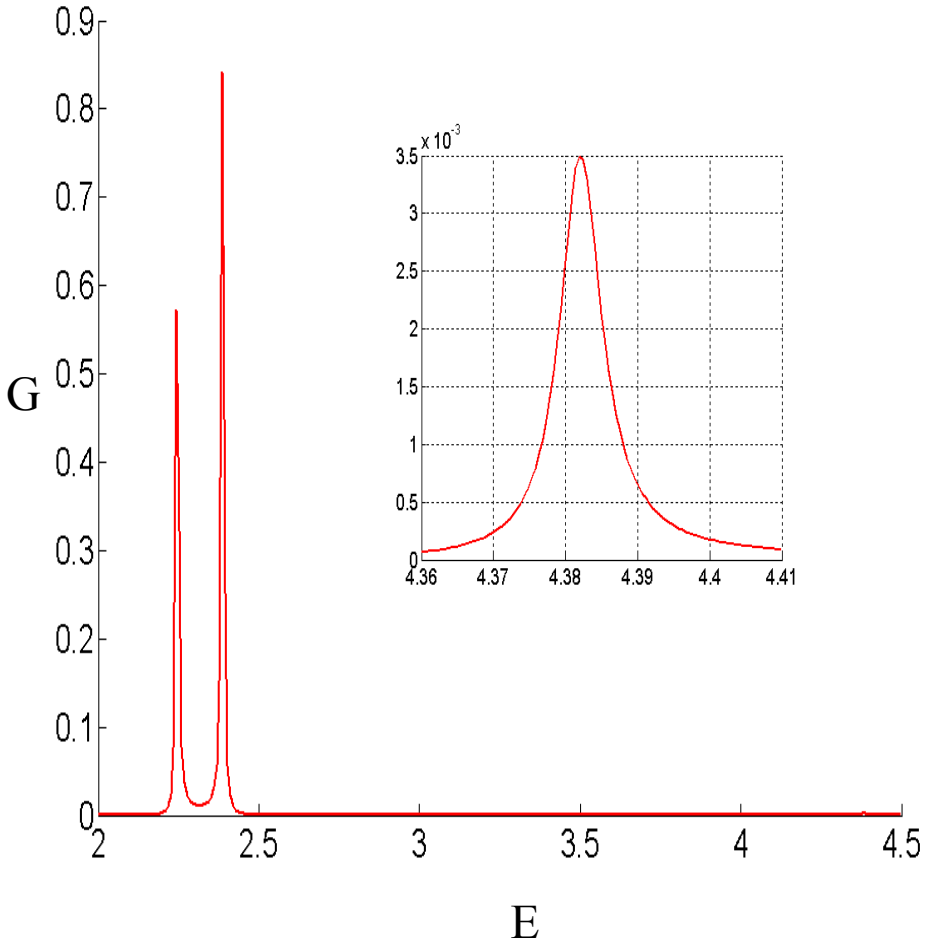


Fig. 5.7: G with unit $2e^2/h$ plotted against energy of incident electron with unit $E_F$ =9meV for $V$= 30 with units $7.12\times10^{-11}$ eV • m to repulsive local potential, zero phonon temperature, width of static barrier 32 nm, phonon energy $\hbar\omega$ = 19.2meV, and mass of phonon $M$ = 1000m$^*$

## The local phonon mass dependence for repulsive local phonon potential at zero phonon temperature

First, In Fig 5.8, the mass of phonon M vary from $100m^*$ to $1000m^*$ and we take the phonon energy $\hbar\omega$=0.74 with unit 9meV, the width of double barrier is ..nm ,the strength of double barrier $V_0$ = 30 with unit $7.12\times10^{-11}$ eV • m and electron-local phonon V= 10 with unit $7.12\times10^{-11}$ eV • m at zero phonon temperature. And the light blue line corresponds to the case of the local phonon replaced by the static barrier with the same strength. In Fig 5.8, the phonon side peaks are also enhanced due the similar reason mentioned above. However, in Fig 5.8, we fixed the wavelength of incident electron wavelength and increase the phonon wavelength from 1.6 nm to 3.2 nm by reducing the mass of phonon from $1000m^*$ to $100m^*$ with the same phonon energy. Second, Fig 5.9 is enlarged Fig 5.8 from E=0.7 to 1.1 with unit 9meV. In Fig 5.9, it is found that as the mass of local become heavier, the main peak become closer to that related to static case.

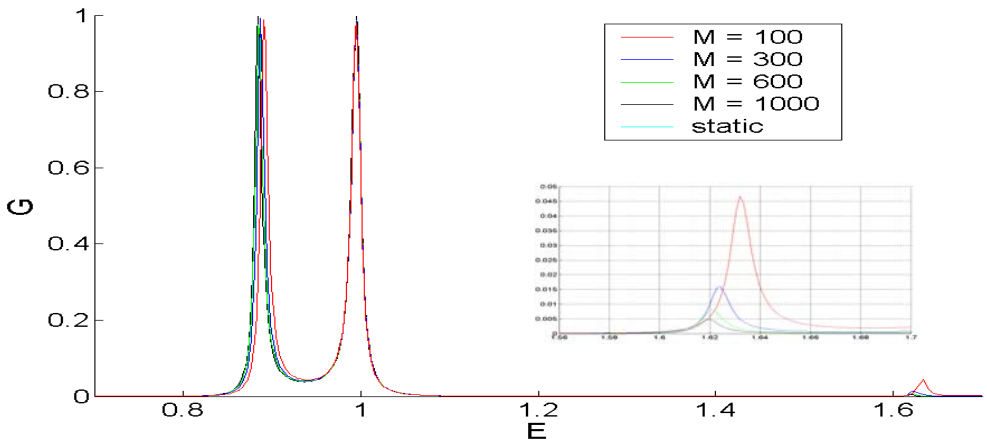


Fig. 5.8: G with unit $2e^2/h$ plotted against energy of incident electron with unit $E_F$ =9meV for $V$= 10 with units $7.12\times10^{-11}$ eV • m to repulsive local potential, zero phonon temperature, width of static barrier 49 nm, phonon energy $\hbar\omega$ = 6.6meV, and mass of phonon $M$ various from $100m^*$ to $1000100m^*$.

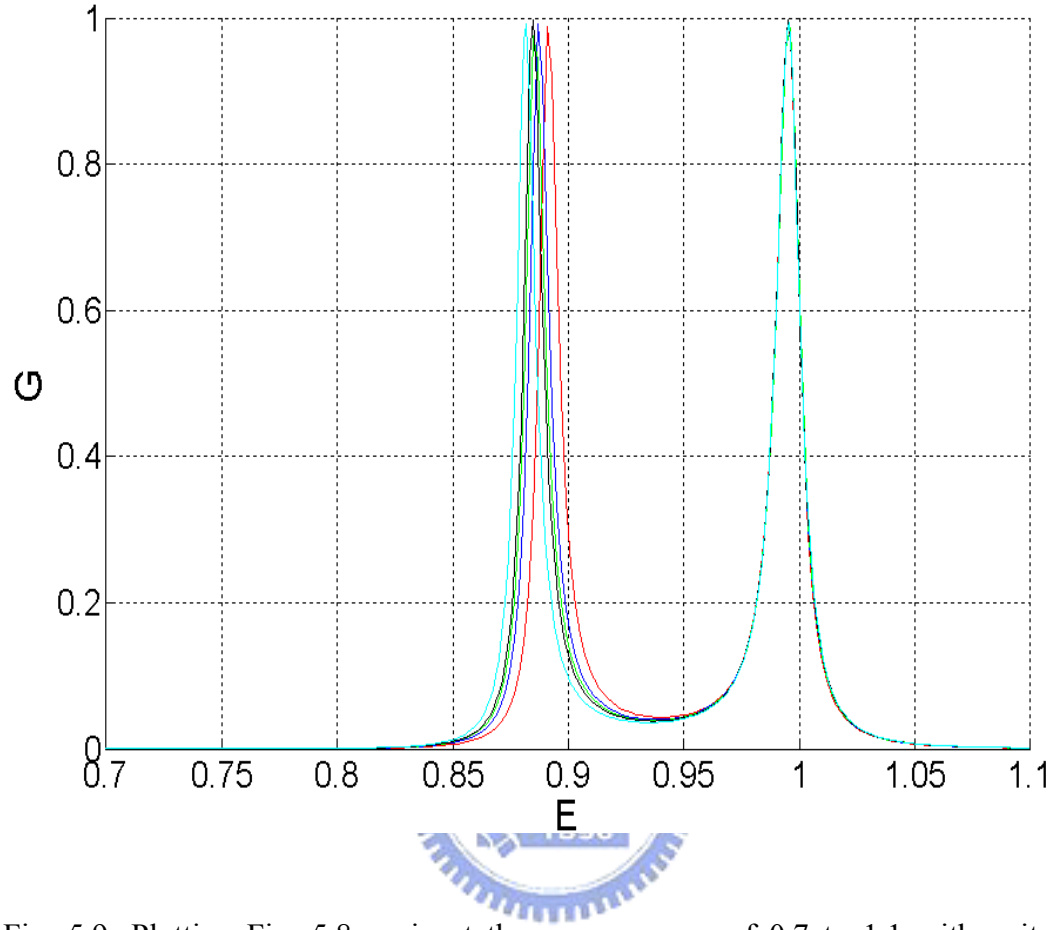


Fig. 5.9: Plotting Fig. 5.8 again at the energy rangy of 0.7 to 1.1 with unit $E_F$ =9meV.

## The electron-local phonon interaction strength dependence for repulsive local phonon potential at zero phonon temperature

In Fig 5.10, the widths of double barrier are respectively W=16 nm and we take the phonon energy ħω=2.14 with unit 9meV, mass of phonon M=1000m$^*$, the strength of double barrier $V_0$ =30 and electron-local phonon V= 8, 10, 20, 25, 30 with unit $7.12\times10^{-11}$ eV・m at zero phonon temperature respectively corresponding to green, blue, red, purple, and black line. In Fig 5.10, we can find that the phonon

sideband peaks cannot be infinitely enhanced by increase the electron-local interaction strength. This is because that the electron wavefunction would be saturated by the local phonon with too strong interaction strength with electron. Therefore, we do not have to enhance the phonon sideband peaks by constantly increasing the interaction strength.

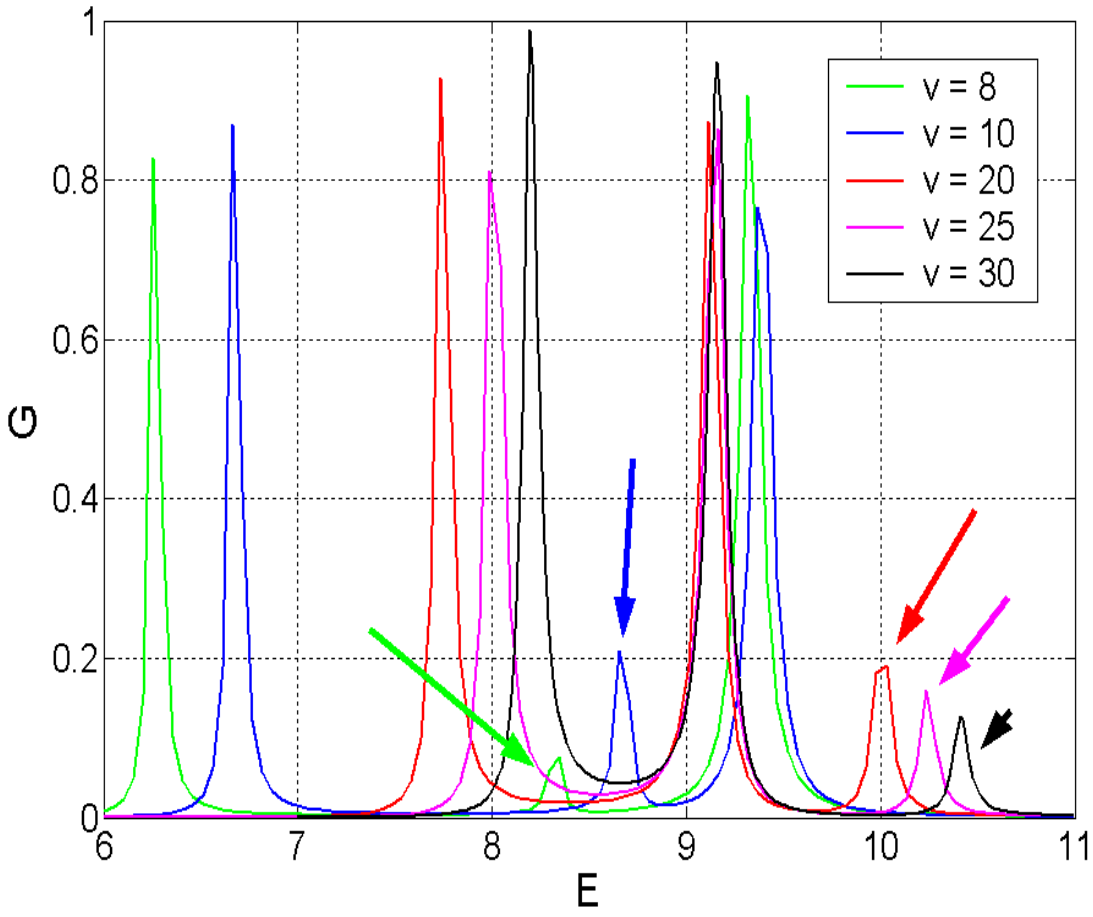


Fig 5.10, the widths of double barrier are respectively W=16 nm and we take the phonon energy ħω=2.14 with unit 9meV, mass of phonon M=1000m$^{*}$, the strength of double barrier $V_0$ =30 and electron-local phonon V= 8, 10, 20, 25, 30 with unit $7.12\times10^{-11}$ eV • m at zero phonon temperature respectively corresponding to green, blue, red, purple, and black line.

## The dependence of the local phonon's oscillation mode n=1 when the electron incident

In Fig 5.11, the widths of double barrier are respectively W=16 nm and we take the phonon energy ħω=2.14 with unit 9meV, mass of phonon M=1000m*, the strength of double barrier $V_0$ =30, electron-local phonon V= 30 with unit $7.12\times10^{-11}$ eV • m and the local phonon staying in n=1 state while the electron incident. In Fig. 5.11, we let the local phonons are excited to the n=1 and 2 states besides of n=0 mode, where we not only see the satellite peaks in the right hand side of the main resonance peak but also in the left hand site due to the electron tunneling through quantum dot resonance level by absorbing a phonon.

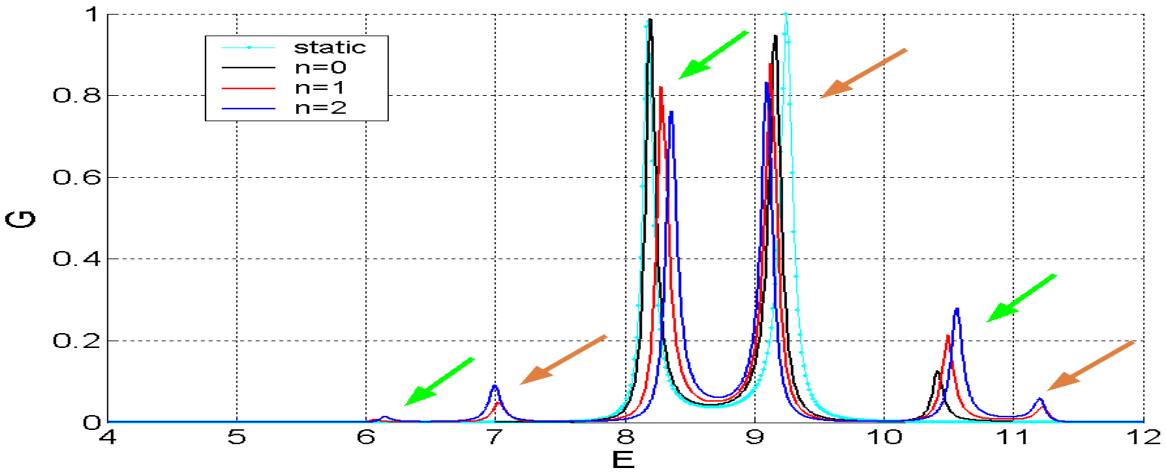


Fig 5.11, The widths of double barrier are respectively W=16 nm and we take the phonon energy ħw=2.14 with unit 9meV, mass of phonon M=1000m*, the strength of double barrier V0 =30, electron-local phonon V= 30 with unit 7.12×10-11 eV • m and the black, red, blue lines respectively corresponding to local phonon staying in n=0, 1, 2 states while the electron incident. Besides, the cyan dot line corresponds to static case.

## Level repulsion phenomenon

In Fig. 5.12 and 5.13, The widths of double barrier are respectively W=16 nm and we take the phonon energy ħw=2.14 with unit 9meV, mass of phonon M=1000m*, and repulsive local phonon potentials' strength V = 8 and V=14 with units $7.12\times10^{-11}$ eV•m respectively to Fig. 5.12 and 5.13. Besides,

red line corresponds to $T_{total.}$ Green line corresponds to $T_{0->0}$+ $T_{0->1->0}$. Black line corresponds to $T_{0->1}$. Cyan line corresponds to local phonon barrier replaced by the same strength static barrier. In Fig 5.12, because the difference of the second and first resonance levels to this system is much larger than the phonon energy. We can separate the main peak due to resonance tunneling through the resonance level of the system and phonon side peak definitely. However, in Fig. 5.14, the difference of the second and first resonance levels to this system is approximately equal to the phonon energy. Therefore, we can see the level repulsion phenomenon.

In summary, we see the phonon sideband peaks due one-phonon emission process expect the main resonance peak due the single molecular quantum dot. Besides, we can enhance the phonon sideband peaks by reducing the wavelength of incident electron.

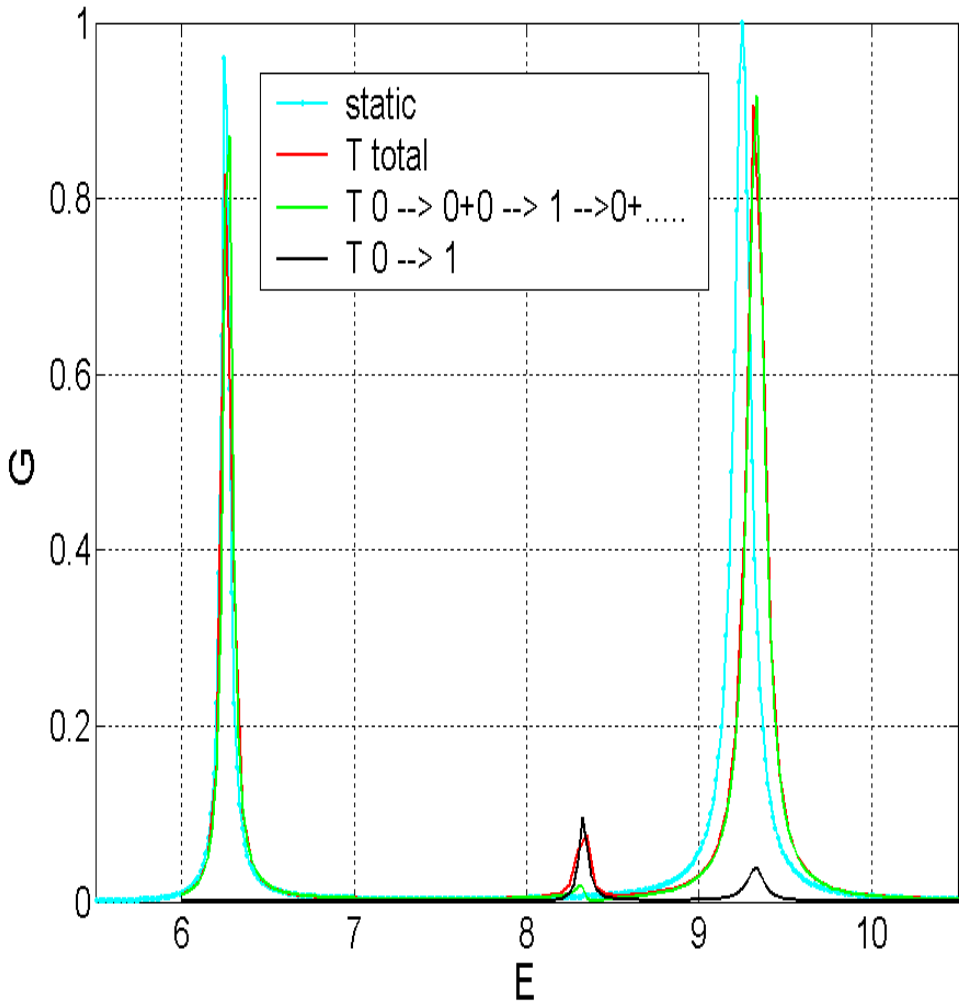


Fig. 5.12 The widths of double barrier are respectively W=16 nm and we take the phonon energy ħw=2.14 with unit 9meV, mass of phonon M=1000m*, and repulsive local phonon potentials' strength V=8 with units $7.12\times10^{-11}$eV • m. Besides, red line corresponds to $T_{total.}$ Green line corresponds to $T_{0->0}$+ $T_{0->1->0}$. Black line corresponds to $T_{0->1}$. Cyan line corresponds to local phonon barrier replaced by the same strength static barrier.

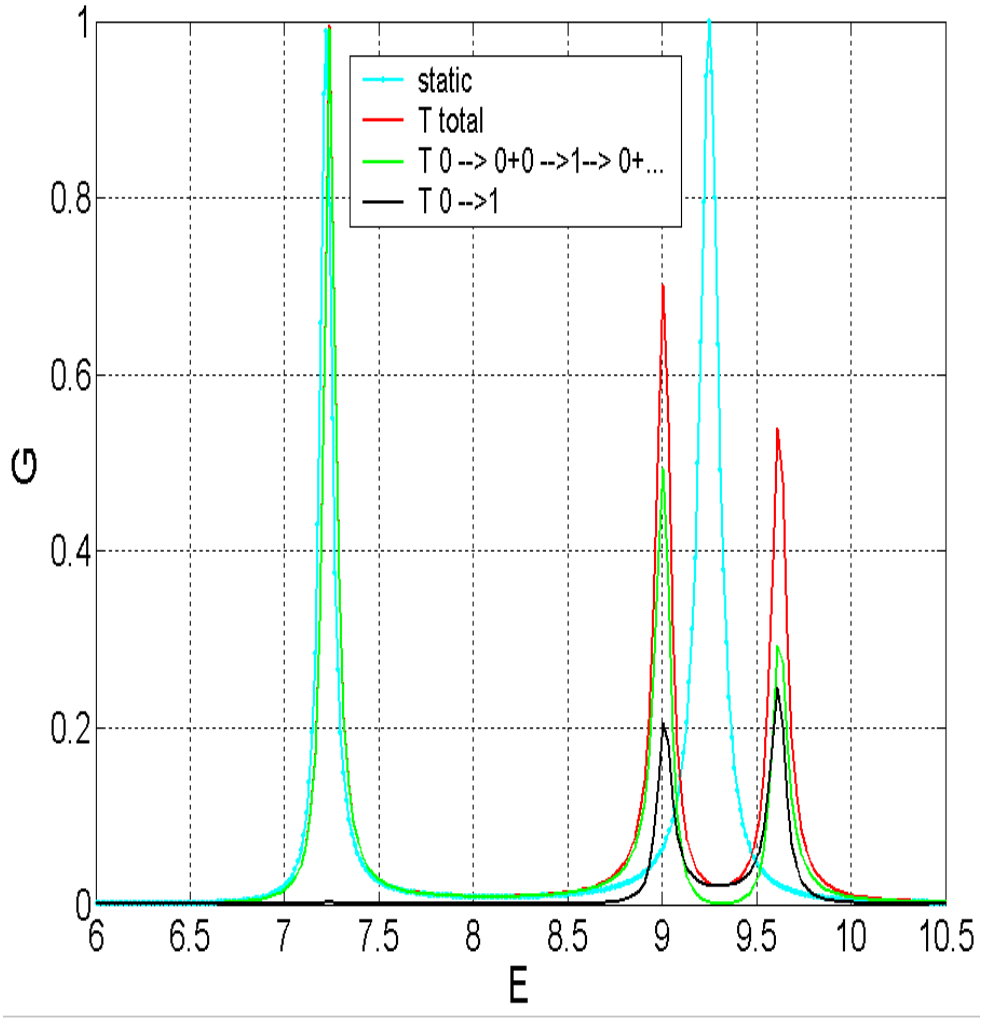


Fig. 5.13 The widths of double barrier are respectively W=16 nm and we take the phonon energy ħw=2.14 with unit 9meV, mass of phonon M=1000m*, and repulsive local phonon potentials' strength V=14 with units $7.12\times10^{-11}$eV • m. Besides, red line corresponds to $T_{total.}$ Green line corresponds to $T_{0->0}$+ $T_{0->1->0}$. Black line corresponds to $T_{0->1}$. Cyan line corresponds to local phonon barrier replaced by the same strength static barrier.

# Chaper 6

# Conclusion remarks

Throughout the thesis, we have developed a non-perturbed method to analyze the effect of local phonons on the electron transport in a 1-D wire as well as the case of quantum dot.

In Ch. 4, we make a complete and detailed analysis to the case of the electron transport in a 1-D wire scattered by local phonons. And our numerical result demonstrate (1) We can see the dip structure in attractive local phonon potential even the mass of phonon up to 1000 times $m^*$. However, in the repulsive local phonon potential , we can find structures in G even the mass of phonon only to 80 times $m^*$, (2) As the temperature increase, the kinks found in conductance G can be thermal averaged,(3) We can find that the transmission coefficient of the propagating electron throughout the local phonons is dominated by the no energy-loss scattering and the one-phonon emission process or one-phonon absorption process has only a little contribution to the transmission coefficient. As mentioned in chap 4, we can find phonon sideband structures in the case of electron transport in a 1-D wire scattered by local phonons but those effects are very small. However, in Ch. 5, we confine electron in the double barrier and succeed to enhance the phonon sideband structures. And, our numerical result demonstrate (1)At zero phonon temperature, we can see the satellite peak on the right side of the resonance peak. Since at zero temperature, no phonon modes are excited on the quantum dot, the propagating electron can tunnel only by emitting a phonon. Therefore, while the phonons modes are excited to the n state on the quantum dot, the satellite peak can also appear on the left hand side of the resonance peak, (2) Even the mass of local phonon is up to 1000 times $m^*$ in repulsive

local phonon potential, the phonon sideband structures can be found obviously only if the electron wavelength is comparable to the phonon wavelength.

Throughout our thesis, we do not really model the single molecule device worked by H. Park. et a*l*.[5]. The model what we use is a single particle model and we can find the interference effects while we neglect the effect of coulomb blockade. That is we neglect the many particle effects. Therefore, in the future, we will try to add the many particle effects to our model.

# Appendix A

To establish an independent check on the about piece-wise mode matching method, we consider the following problem. It is an infinite long wire of width w=2 with a hard wall confinement an a barrier at $y=y_0$ exist within the region 0 =< x <= $L$ as shown in Fig. A1.

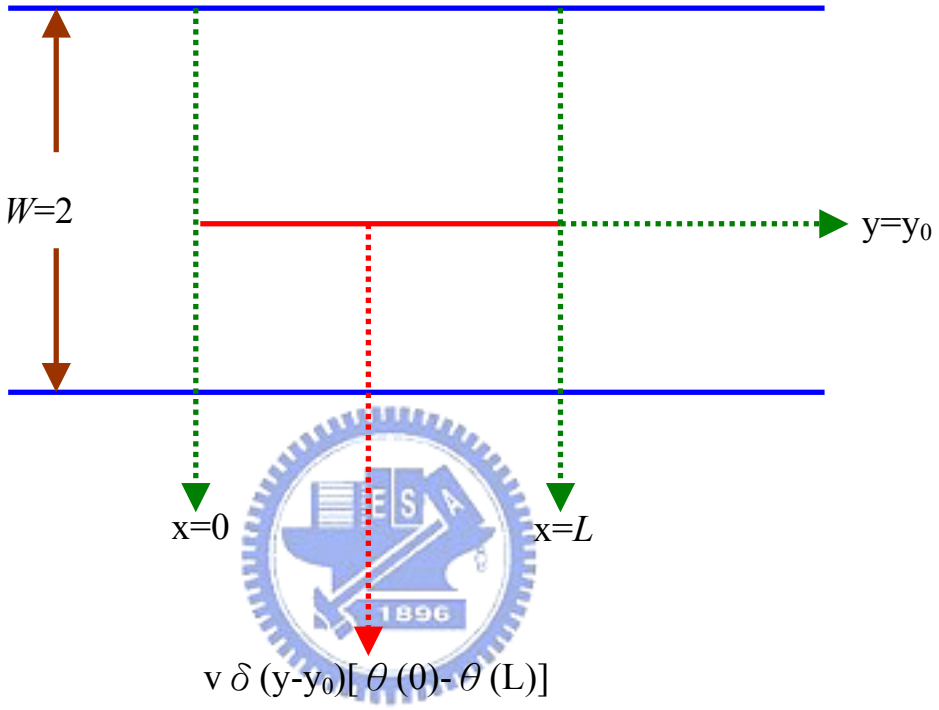


Fig. A1 An infinite long wire of width w=2 with a hard wall confinement an a barrier at $y=y_0$ exist within the region 0 =< x <= $L$. The Hamilton can be written as

$$H = -\frac{\hbar^2}{2m}\frac{\partial^2}{\partial x^2} + H.W + v\delta(y - y_0)[\theta(0) - \theta(L)] \qquad \text{(A1)}$$

This problem allows another method of calculation which we mode match at x=0 and x=L only. And we can make sure the correctness of the scattering matrix method by this way.

# Bibliography


[1] T.Stauber, R.Zimmermenn, and H. Castella, Phys. Rev. B **62**, 7336(2000).

[2] B.Y. Gelfand, S. Schmitt-Rink, and A.F.J. Levi, Phys. Rev. Lett. **62**, 1683(1989)

[3] P.F. Bagwell, Phys. Rev. B **41,** 10354(1990)

[4] M. A. Reed, C. Zhou, C.J. Muller, T.P. Burgin, and J.M. Tour, Science **278**, 252 (1997).

[5] H. Park, J. Park, A. K. L. Lim, E. H. Anderson, A. P. Alivisatos, and P. L. McEuen, Nature (London) **407**, 57(2000)

[6] J. Park et a*l*., Nature (London) **417**, 722 (2002).

[7] W. Liang, M. P. Shores, M. Bockrath, J. R. Long, and H. Park, Nature(London) **417**, 725(2002).

[8] R. H. M. Smit, Y. Noat, C. Untiedt, N. D. Lang, M. C. van Hermert, and J. M. van Ruitenbeek, Nature (London) **419**, 906(2002).

[9] N. B. Zhitenev, H. Meng, and Z. Bao, Phys. Rev. Lett. **88**, 226801 (2002).

[10] Jian-Xin Zhu and A. V. Balatsky, Phys. Rev. B **67**, 165326(2000).

[11] D. A. Ryndyk* and J. Keller, Phys. Rev. B **71**, 073305 (2005).

[12] B. J. van Wees, H. van Houton, C. W. J. Beenakker, J. G. Williamson, L. P. Kouwenhoven, D. van der Marel, and C.T. Foxon, Phys. Rev. Lett **60**, 848 (2005).

[13] D. A. Wharam, T. J. Thornton, R. Newbery, M. Pepper, H. Ahmed, J. E. F. Forst, D. G. HasKo, D. C. Peacock, D. A. Ritchie, and G. A. C. Jones, J., Phys. C **21**, L209 (1988).

[14] Klein, D. L. McEuen, P.L. Bowen Katari, J. E. Roth, R. & Alivisatos, A. P. Appl. Phys. Lett. **68**, 2574-2576 (1996).

[15] Klein, D. L. Roth, R. Lim, A. K. L. Alivisatos, A. P. & MuEuen, P. L., Nature **389**,699-701 (1997).

[16] Park, H. Lim, A. K. L. Prak, J. Alivisatos, A. P. & MuEuen, P. L., Appl. Phys. Lett. **75**, 301-303 (1999).

[17] Banin, U. Cao. Y. Kaz., D. & Millo. O., Nature **400**, 542-544 (1999).

[18] Klim, S.-H., Medeiros-Ribeiro, G. ohlberg, D. A. A. Williams, R.S. & Health, J. R. Phys. Chem. B. **103**, 10341-10347 (1999).

[19] Bockrath, M. et a*l.* Science **275**, 1922-1925 (1997).

[20] Tans, S. J. et a*l*. Nature 386,474-477 (1997).

[21] M. Büttiker et. a*l*., Phys. Rev. Lett. **57**, 1761 (1986).

[22] A.Szafer and A.D. Stone, Phys. Rev. Lett., **62**, 300 (1989).